A water-soluble iron-porphyrin complex capable of rescuing CO-poisoned red blood cells

Daniel G. Droege and Timothy C. Johnstone *

Department of Chemistry and Biochemistry, University of California, Santa Cruz, California 95064, United States.

ABSTRACT We describe herein a small-molecule platform that exhibits key properties needed by an antidote for CO poisoning. The design features an iron-porphyrin complex with bulky substituents above and below the macrocyclic plane to provide a hydrophobic pocket for CO binding and to prevent the formation of inactive oxo-bridged dimers. Peripheral charged groups impart water solubility. We demonstrate that the Fe(II) complex of a porphyrin with 2,6-diphenyl-4-sulfo-phenyl *meso* substituents can bind CO, stoichiometrically sequester CO from carboxyhemoglobin, and rescue CO-poisoned red blood cells.

Carbon monoxide is celebrated as an endogenous gasotransmitter and low doses of CO have demonstrated salutary effects in health conditions ranging from cancer to coronary heart disease.[1] Nevertheless, high levels of CO exposure are harmful and the toxicity of CO is attributed in part to its ability to bind hemoglobin (Hb), forming carboxyhemoglobin (COHb) and inhibiting O_2 transport.[2] Hb binds CO approximately 200-250-fold more strongly than O_2, and the distinctively red-shifted Soret band of COHb is used clinically to assess CO exposure.[3,4]

In the United States alone, over 50,000 emergency department visits each year are attributed to CO exposure.[5] Despite the prevalence of CO poisoning, there is no clinically-approved antidote available. Current best practices involve placing the afflicted individual in fresh air, delivering 100% O_2, or administering superatmospheric levels of O_2 in a hyperbaric chamber.[6] The typical half-life of COHb in the bloodstream is 5.3 h, but hyperbaric O_2 (1.5-3 atm) can decrease this half-life to < 1 h.[7] Unfortunately, these large chambers are generally located in tertiary care centers to which patients must be transported. Moreover, hospitals typically house only a few such chambers, which could be rapidly overwhelmed in the event of a mass exposure.

We appreciate, therefore, that there is a pressing need for a rapid and effective antidote for CO poisoning. An important recent development in this area was the discovery that a mutant form of neuroglobin can function as a CO-poisoning antidote.[8-10] The supramolecular hemoCD complexes formed from iron(II) porphyrins and modified cyclodextrins have also demonstrated a high affinity for CO.[11] The chemistry of these compounds has been exploited to probe CO physiology,[12-15] and could also have utility in binding toxic molecules.[16] Finally, a series of synthetic peptides has been explored for their ability to allosterically enhance the release of CO from COHb.[17] We sought to develop a modular small-molecule platform that exploits the CO-affinity of Fe(II) porphyrin compounds. We have prepared a proof-of-principle compound that

forms a strong CO adduct and we demonstrate that this affinity allows it to stoichiometrically remove CO from COHb. Moreover, we demonstrate that this compound can rescue CO-poisoned red blood cells (RBCs) by quantitatively sequestering CO while leaving the cells intact.

Our design is inspired by the seminal bioinorganic studies on picket-fence porphyrins,[18-19] which bind CO more strongly than O_2.[20] Steric bulk can prevent the formation of deactivated μ-oxo species, but the atropisomeric purity of the original picket-fence porphyrins is unnecessary for CO sequestration. We turned, therefore, to symmetrically substituted bis-pocket porphyrins featuring 2,6-disubstituted *meso*-phenyl groups.[21] We reasoned that the 4-position of the *meso*-phenyl unit could be functionalized with a charged group to impart water solubility (Figure 1A). We emphasize that the large, highly charged complex will have limited-to-no cellular uptake by design; cellular uptake is not required because the complex will not need to interact directly with COHb to function. We stress that the thermodynamic stability of COHb does not preclude kinetic lability, which has been exploited to transfer CO between heme proteins.[8] If a metalloporphyrin complex has a CO affinity sufficiently greater than that of Hb, transfer will proceed (Figure 1B).

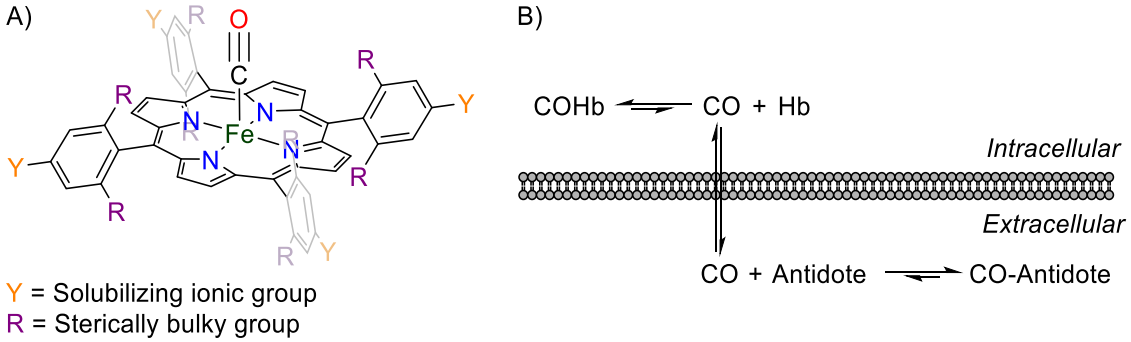

Fig. 1 A) Schematic overview of the proposed small-molecule for CO sequestration. B) Proposed mechanism of action.

To validate our design, we targeted the synthesis of iron-porphyrin complex **6** with 2,6-diphenyl-4-sulfophenyl *meso* substituents (Scheme 1). The *ortho*-phenyl groups will prevent μ-oxo dimer

formation and create a hydrophobic CO-binding pocket. The *para*-sulfonate groups will ensure water solubility at physiological pH. The bis-pocket porphyrin with 2,4,6-triphenylphenyl *meso* substituents was previously accessed from pyrrole and 2,4,6-triphenylbenzaldehyde using a standard Adler synthesis, but macrocyclization was inhibited by the extreme steric congestion in the product; the final yield was 1%.[21] We instead targeted 2,6-dibromophenyl-containing *meso* substituents so that steric bulk can be incorporated via Pd-catalyzed cross-coupling reactions *after* macrocyclization. Finally, we avoided the complications associated with harsh electrophilic aromatic sulfonation by incorporating a trimethylsilyl group that can undergo facile late-stage conversion to a sulfonyl chloride, which can then be hydrolyzed to a sulfonate.[22]

(3,5-Dibromophenyl)trimethylsilane (**1**) was prepared from 1,3,5-tribromobenzene via sequential reaction with *n*-BuLi and Me_3SiCl. Conversion to aldehyde **2** was achieved via deprotonation with LDA and carbonylation with DMF. $BF_3{\cdot}OEt_2$-catalyzed condensation of **2** and pyrrole proceeded readily to give brominated porphyrin **3**, which is sparingly soluble in MeCN. Washing the crude product with MeCN until the filtrate is colorless afforded analytically pure material in 48% yield. Eight phenyl rings were installed on the porphyrin via Suzuki-Miyaura coupling in 20:1 1,4-dioxane/water using a three-fold excess of $PhB(OH)_2$ (per Ar–Br bond), Cs_2CO_3 as a base, and 12.5 mol% $(dppf)PdCl_2$ (per Ar–Br bond). Silica gel chromatography afforded bulky porphyrin **4** as a deep purple solid in 86% yield. Single-crystal X-ray diffraction confirms the formation of the desired hydrophobic pocket (Figure S20).

Iron was inserted into **4** by refluxing it with $Fe(CO)_5$ and a catalytic amount of I_2 in toluene under N_2 for 4 h; an additional hour of reflux in open air followed by an alkaline aqueous work-up ensured oxidation to the Fe(III) state. ^{1}H NMR spectroscopy in $CDCl_3$ confirms that product **5** is paramagnetic, with broadened phenyl resonances appearing in the 15-20 ppm range and the β-

pyrrole protons characteristically resonating at 82.16 ppm.[23] Crystals of the reaction product grown from MeCN confirmed the proposed connectivity and the presence of an apical hydroxide ligand (Figure S21).

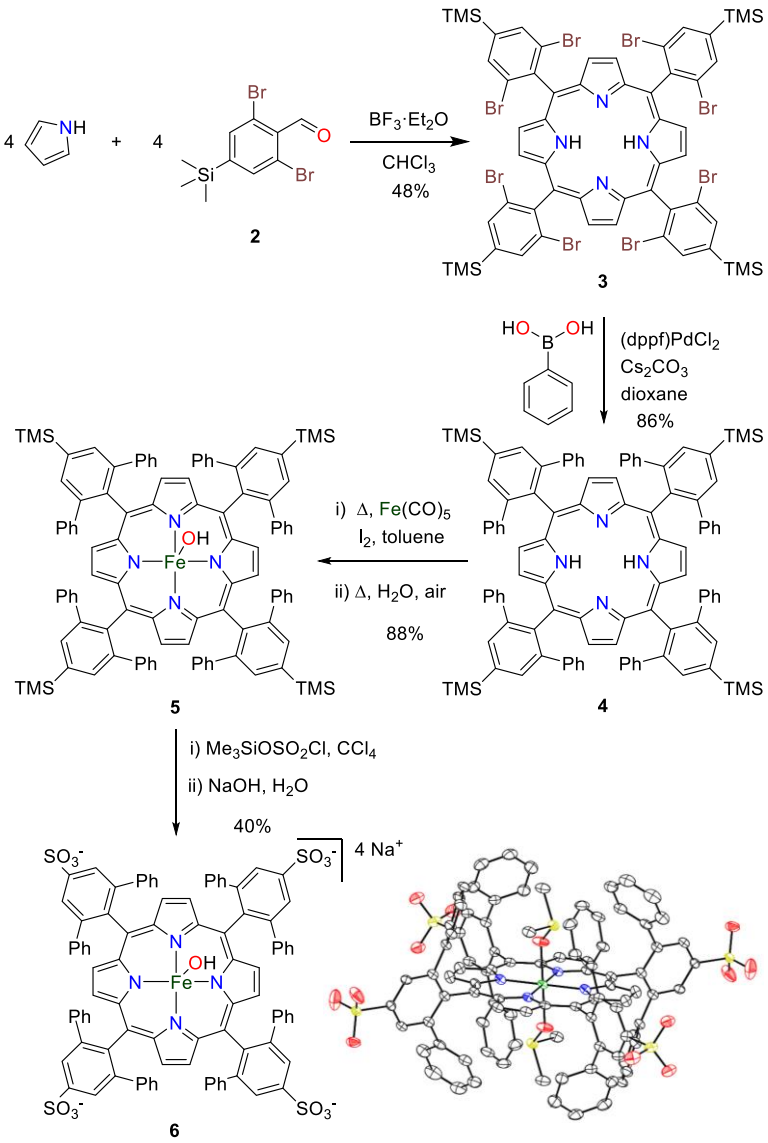

Scheme 1 Synthesis of **6** (details provided in ESI) and molecular structure (50% ellipsoids) of the anion obtained upon slow recrystallization of **6** from DMSO/$CHCl_3$. H atoms, solvent, and counterions omitted for clarity. Color code: Fe green, O red, S yellow, N blue, C grey.

Compound **5** was treated with Me_3SiOSO_2Cl in CCl_4 followed by hydrolysis with 1 M NaOH(aq). The intensely colored porphyrin complex was extracted from the reaction mixture with water and subsequently purified by reverse-phase chromatography. The final tetrasodium salt **6** was isolated as a very dark purple solid in 40% yield. The purity of the product was established using analytical HPLC (Figure S16). Weakly diffracting crystals confirmed the proposed connectivity, including the apical hydroxide ligand (Figure S22). High-quality crystals that were grown from DMSO/$CHCl_3$ permitted atomic-resolution refinement that confirmed the proposed structure, albeit following axial ligand substitution (Scheme 1). In the crystal, the complex sits on an inversion center and, although planarity of the ligand is not crystallographically required, the RMSD of the atoms of the porphyrin core from the plane of best fit is only 0.024 Å.

Compound **6** (λ_{max} = 431 nm in PBS, pH 7.4) can be reduced *in situ* using $Na_2S_2O_4$ to afford an Fe(II) complex (Figure 3). Upon reduction, the Soret band red shifts to 448 nm (Figure 3B), consistent with reduction to an Fe(II) porphyrin.[11] The ^{1}H NMR spectrum of the *in situ* generated reduction product in deuterated PBS (PBS-*d*) exhibits a signal at –3.63 ppm, which we tentatively assign as the β-pyrrole protons, and Evans' method measurements return a μ_{eff} of 3.69 μ_B (Figure S14). These data are consistent with the formation of a four-coordinate intermediate-spin (S = 1) Fe(II) complex.[24-26] We highlight that an anomalously high μ_{eff}, as compared to the predicted spin-only magnetic moment for an intermediate-spin Fe(II) porphyrin, has also been reported for Fe(TPP) and has been rationalized in terms of spin-orbit coupling.[27]

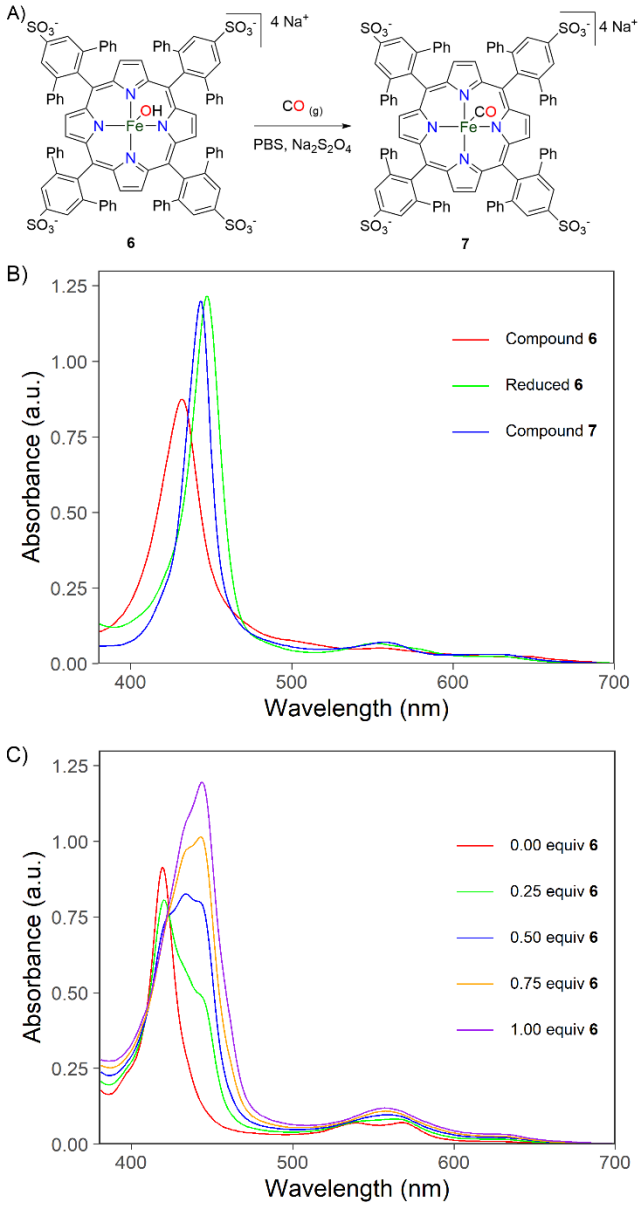

Fig. 3 A) Reaction of **6** with CO under reducing conditions to produce **7**. B) Electronic absorption spectra of 10 μM solutions of **6**, reduced **6**, and **7** in PBS (pH 7.4). For reduced **6** and **7**, the solutions also contain 5.7 mM $Na_2S_2O_4$. C) Titration of bovine COHb (2.5 μM) with **6** in PBS (pH 7.4, 5.7 mM $Na_2S_2O_4$).

Under an inert atmosphere, PBS solutions of this Fe(II) complex containing $Na_2S_2O_4$ are stable for days. When the solutions are opened to air, the complex reverts to **6** ($t_{½} \approx 30$ min)

following aerial oxidation of the dithionite (Figure S17). Addition of CO to solutions of reduced **6** produces the CO adduct **7** (Figure 3A). Compound **7** is characterized by a Soret band at 444 nm in PBS (Figure 3B); this hypsochromic shift is consistent with formation of an Fe(II)–CO complex.[11] In PBS, solutions of **7** that have been opened to air revert to **6** with $t_{½} \approx 120$ min (Figure S18). If the reduction of **6** under a CO atmosphere is performed in PBS-*d*, ^{1}H NMR spectroscopy clearly shows **7** to be diamagnetic and Evans' method measurements return a μ_{eff} of 0 μ_B (Figure S15). These results are consistent with the formation of a low-spin Fe(II) complex, which would be expected upon complexation of CO. Salt metathesis, effected by addition of excess $(Ph_4P)Cl$ to an aqueous solution of **7**, results in rapid precipitation of a red solid. IR spectroscopic analysis of this solid revealed a ν_{CO} of 1970 cm^{-1} (Figure S19). The higher value of ν_{CO} for **7** as compared to COHb (1951 cm^{-1})[28] suggests that the small-molecule porphyrin complex will bind CO more strongly than Hb.[20] This prediction was tested by titrating COHb with **6** in PBS under reducing conditions (5.7 mM $Na_2S_2O_4$). We observed a dose-dependent and stoichiometric transfer of CO to form **7** and deoxyHb with tight isosbestic points, indicating a clean transition from COHb to (deoxyHb + **7**) (Figure 3C). The stoichiometric transfer with each aliquot reveals that the CO binding constant is appreciably greater than that of Hb ($P_{½}^{CO} < 0.004$ torr).[20] We also titrated a solution of deoxyHb and **6** in 5.7 mM $Na_2S_2O_4$ with CO-saturated water. The first equivalent of CO converts reduced **6** to **7** but leaves deoxyHb unchanged. Addition of a second equivalent of CO results in conversion of deoxyHb to COHb (Figure S23). These experiments confirm that reduced **6** can bind CO preferentially in the presence of Hb and sequester CO from COHb. Although characterization of the kinetics of CO binding will be the topic of future studies, we note that in these experiments, all changes were complete between the time of mixing and spectral acquisition (20-30 s). We also note that titration of a 5.7 mM $Na_2S_2O_4$ solution of COHb with

5,10,15,20-tetrakis(4-sulphonatophenyl)porphyrinatoiron(III), i.e. the derivative of **6** in which the phenyl groups above and below the porphyrin plane are replaced with H atoms, does not result in CO transfer (Figure S24).

Finally, we tested whether reduced **6** could sequester CO from poisoned bovine RBCs after confirming that it does not induce hemolysis (Figure S25). We performed our spectroscopic titrations directly on suspensions of CO-treated RBCs in PBS containing 5.7 mM dithionite. We note that the intensity of the Soret band of COHb (λ_{max} = 420 nm) is decreased from the concentration-predicted absorbance because of an inner filter effect introduced by concentration of the Hb into the RBCs. Accurate concentrations of COHb were obtained by measuring the absorbance of lysed aliquots of the suspension. Titration of the cell suspension with **6**, which is reduced *in situ*, resulted in a dose-dependent decrease in the intensity of the COHb signal, and an increase of the signal for **7** (λ_{max} = 444 nm) (Figure 4). To confirm that CO had indeed been abstracted from Hb, additional CO was bubbled through the suspension of RBCs that had been treated with 1 equiv of **6**; the COHb signal was regenerated. Although a detailed analysis of the kinetics of CO transfer and sequestration will be the subject of future work, we gained preliminary insight by monitoring absorbance at 420 nm of a quiescent suspension of CO-poisoned RBCs in a buffered dithionite solution following addition of 1 equiv of **6**. The reaction was essentially complete within 3 min (Figure S26).

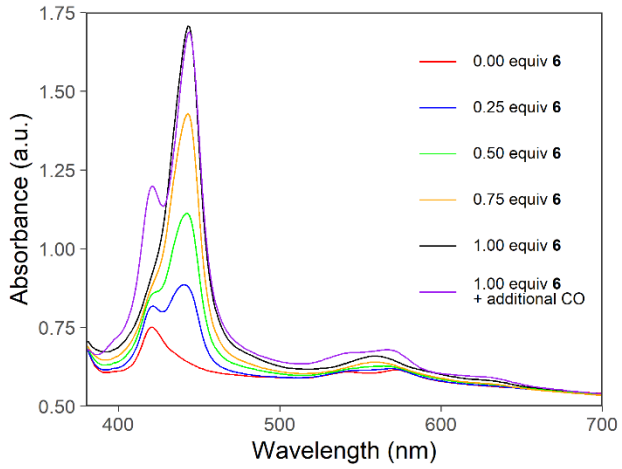

Fig. 4 Titration of a PBS suspension (pH 7.4, 5.7 mM $Na_2S_2O_4$) of CO-treated bovine RBCs with **6** (reduced *in situ*). Final trace obtained after bubbling CO through the suspension treated with 1.00 equiv of **6**.

We note that Fe-porphyrin compounds have been observed to bind 2 equiv of CO,[29] but our titration experiments reveal that CO transfer from COHb to reduced **6** occurs to form **7** with a 1:1 stoichiometry and that no change in the UV-vis spectrum of **7** is observed under 1 atm CO. Moreover, the ν_{CO} of **7** (1970 cm^{-1}) agrees much better with that of FeTPP(CO) (1973 cm^{-1}) than that of $FeTPP(CO)_2$ (2042 cm^{-1}), where TPP = tetraphenylporphyrin.[29] The UV-vis spectrum of **7** also agrees better with FeTPP(CO) than $FeTPP(CO)_2$. These results indicate that **7** is a monocarbonyl complex.

In summary, we have reported the design of a small-molecule platform for CO sequestration that could have applications in the development of a CO-poisoning antidote. A proof-of-principle compound, **6**, has demonstrated the viability of the synthetic strategy. Upon reduction, **6** has an affinity for CO, an ability to remove CO from COHb, and the capacity to sequester CO from poisoned RBCs. This activity is performed without any damage to the cells. The increased affinity of reduced **6** for CO as compared to Hb is expected to arise from a combination of

increased electron density at the metal center, increased hydrophobicity of the CO-binding pocket, and decreased steric hinderance to linear binding; ongoing studies with the derivatives that can be readily accessed from **3** will shed light on the relative importance of these factors. We are continuing to investigate derivatives of **6** to uncover compounds with the greater stability, selectivity, and O_2 tolerance needed to function as CO-poisoning antidotes.

We thank the Hellman Foundation for awarding a Hellman Fellowship to T.C.J. and the UCSC Committee on Research for a Special Research Project Grant. X-ray diffraction studies were performed on an instrument purchased with NSF MRI grant #2018501. MALDI-TOF experiments were performed with assistance from Gordon T. Luu and Prof. Laura M. Sanchez using instrumentation supported by UCSC start-up funds to L.M.S.

There are no conflicts to declare.

REFERENCES

1. Motterlini, R.; Foresti, R., Biological signaling by carbon monoxide and carbon monoxide-releasing molecules. *Am. J. Physiol.: Cell Physiol.* **2017,** *312*, C302-C313.

2. Roderique, J. D.; Josef, C. S.; Feldman, M. J.; Spiess, B. D., A modern literature review of carbon monoxide poisoning theories, therapies, and potential targets for therapy advancement. *Toxicology* **2015,** *334*, 45-58.

3. Rodkey, F. L.; Hill, T. A.; Pitts, L. L.; Robertson, R. F., Spectrophotometric measurement of carboxyhemoglobin and methemoglobin in blood. *Clin. Chem.* **1979,** *25*, 1388-1393.

4. Stewart, R. D., The Effect of Carbon Monoxide on Humans. *Annu. Rev. Pharmacol.* **1975,** *15*, 409-423.

5. Sircar, K.; Clower, J.; Shin, M. k.; Bailey, C.; King, M.; Yip, F., Carbon monoxide poisoning deaths in the United States, 1999 to 2012. *Am. J. Emerg. Med.* **2015,** *33*, 1140-1145.

6. Hampson, N. B.; Piantadosi, C. A.; Thom, S. R.; Weaver, L. K., Practice Recommendations in the Diagnosis, Management, and Prevention of Carbon Monoxide Poisoning. *Am. J. Respir. Crit. Care Med.* **2012,** *186*, 1095-1101.

7. Weaver, L. K.; Deru, K., Carboxyhemoglobin half-life during hyperbaric oxygen in a patient with lung dysfunction: a case report. *Undersea Hyperbaric Med.* **2017,** *44*, 173-177.

8. Azarov, I.; Wang, L.; Rose, J. J.; Xu, Q.; Huang, X. N.; Belanger, A.; Wang, Y.; Guo, L.; Liu, C.; Ucer, K. B.; McTiernan, C. F.; Odonnell, C. P.; Shiva, S.; Tejero, J.; Kim-Shapiro, D. B.; Gladwin, M. T., Five-coordinate H64Q neuroglobin as a ligand-trap antidote for carbon monoxide poisoning. *Sci. Transl. Med.* **2016,** *8*, 368ra173.

9. Rose, J. J.; Bocian, K. A.; Xu, Q.; Wang, L.; DeMartino, A. W.; Chen, X.; Corey, C. G.; Guimarães, D. A.; Azarov, I.; Huang, X. N.; Tong, Q.; Guo, L.; Nouraie, M.; McTiernan, C. F.; O'Donnell, C. P.; Tejero, J.; Shiva, S.; Gladwin, M. T., A neuroglobin-based high-affinity ligand trap reverses carbon monoxide–induced mitochondrial poisoning. *J. Biol. Chem.* **2020,** *295*, 6357-6371.

10. Rydzewski, J.; Nowak, W., Photoinduced transport in an H64Q neuroglobin antidote for carbon monoxide poisoning. *J. Chem. Phys.* **2018,** *148*, 115101.

11. Kano, K.; Kitagishi, H.; Kodera, M.; Hirota, S., Dioxygen Binding to a Simple Myoglobin Model in Aqueous Solution. *Angew. Chem., Int. Ed.* **2005,** *44*, 435-438.

12. Kitagishi, H.; Negi, S.; Kiriyama, A.; Honbo, A.; Sugiura, Y.; Kawaguchi, A. T.; Kano, K., A Diatomic Molecule Receptor That Removes CO in a Living Organism. *Angew. Chem., Int. Ed.* **2010,** *49*, 1312-1315.

13. Kitagishi, H.; Minegishi, S.; Yumura, A.; Negi, S.; Taketani, S.; Amagase, Y.; Mizukawa, Y.; Urushidani, T.; Sugiura, Y.; Kano, K., Feedback Response to Selective Depletion of Endogenous Carbon Monoxide in the Blood. *J. Am. Chem. Soc.* **2016,** *138*, 5417-5425.

14. Minegishi, S.; Yumura, A.; Miyoshi, H.; Negi, S.; Taketani, S.; Motterlini, R.; Foresti, R.; Kano, K.; Kitagishi, H., Detection and Removal of Endogenous Carbon Monoxide by Selective and Cell-Permeable Hemoprotein Model Complexes. *J. Am. Chem. Soc.* **2017,** *139*, 5984-5991.

15. Kitagishi, H.; Minegishi, S., Iron(II)porphyrin–Cyclodextrin Supramolecular Complex as a Carbon Monoxide-Depleting Agent in Living Organisms. *Chem. Pharm. Bull.* **2017,** *65*, 336-340.

16. Kitagishi, H.; Kano, K., Synthetic heme protein models that function in aqueous solution. *Chem. Commun.* **2021,** *57*, 148-173.

17. Goldstein, S. R.; Liu, C.; Safo, M. K.; Nakagawa, A.; Zapol, W. M.; Winkler, J. D., Design, Synthesis, and Biological Evaluation of Allosteric Effectors That Enhance CO Release from Carboxyhemoglobin. *ACS Med. Chem. Lett.* **2018,** *9*, 714-718.

18. Collman, J. P.; Gagne, R. R.; Halbert, T. R.; Marchon, J.-C.; Reed, C. A., Reversible oxygen adduct formation in ferrous complexes derived from a "picket fence" porphyrin. A model for oxymyoglobin. *J. Am. Chem. Soc.* **1973,** *95*, 7868-7870.

19. Collman, J. P.; Gagne, R. R.; Reed, C.; Halbert, T. R.; Lang, G.; Robinson, W. T., "Picket fence porphyrins." Synthetic models for oxygen binding hemoproteins. *J. Am. Chem. Soc.* **1975,** *97*, 1427-1439.

20. Collman, J. P.; Brauman, J. I.; Halbert, T. R.; Suslick, K. S., Nature of O2 and CO binding to metalloporphyrins and heme proteins. *Proc. Natl. Acad. Sci. U.S.A.* **1976,** *73*, 3333-3337.

21. Suslick, K. S.; Fox, M. M., A Bis-Pocket Porphyrin. *J. Am. Chem. Soc.* **1983,** *105*, 3507-3510.

22. Ye, B. H.; Naruta, Y., A novel method for the synthesis of regiospecifically sulfonated porphyrin monomers and dimers. *Tetrahedron* **2003,** *59*, 3593-3601.

23. La Mar, G. N.; Walker, F. A., Dynamics of Axial Ligation in Metalloporphyrins. I. Imidazole Exchange in Low-Spin Ferric Porphyrins. *J. Am. Chem. Soc.* **1972,** *94*, 8607-8608.

24. Walker, F. A., NMR and EPR Spectroscopy of Paramagnetic Metalloporphyrins and Heme Proteins. In *Handbook of Porphyrin Science (Volume 6)*, 2010; pp 1-337.

25. Collman, J. P.; Hoard, J. L.; Kim, N.; Lang, G.; Reed, C. A., Synthesis, stereochemistry, and structure-related properties of α,β,γ,δ-tetraphenylporphinatoiron(II). *J. Am. Chem. Soc.* **1975,** *97*, 2676-2681.

26. Hu, C.; Noll, B. C.; Schulz, C. E.; Scheidt, W. R., Four-Coordinate Iron(II) Porphyrinates: Electronic Configuration Change by Intermolecular Interaction. *Inorg. Chem.* **2007,** *46*, 619-621.

27. Tarrago, M.; Römelt, C.; Nehrkorn, J.; Schnegg, A.; Neese, F.; Bill, E.; Ye, S., Experimental and Theoretical Evidence for an Unusual Almost Triply Degenerate Electronic Ground State of Ferrous Tetraphenylporphyrin. *Inorg. Chem.* **2021,** *60*, 4966-4985.

28. Moore, J. N.; Hansen, P. A.; Hochstrasser, R. M., Iron-carbonyl bond geometries of carboxymyoglobin and carboxyhemoglobin in solution determined by picosecond time-resolved infrared spectroscopy. *Proc. Natl. Acad. Sci. U.S.A.* **1988,** *85*, 5062-5066.

29. Wayland, B. B.; Mehne, L. F.; Swartz, J., Mono- and biscarbonyl complexes of iron(II) tetraphenylporphyrin. *J. Am. Chem. Soc.* **1978,** *100*, 2379-2383.

Electronic Supplementary Information for

A water-soluble iron-porphyrin complex capable of rescuing CO-poisoned red blood cells

*Daniel G. Droege and Timothy C. Johnstone**

Department of Chemistry and Biochemistry, University of California, Santa Cruz, California 95064, United States.

* Correspondence to: johnstone@ucsc.edu

CONTENTS

Experimental Methods

General considerations. All reactions were performed under N_2 unless otherwise stated. Glassware was oven dried prior to use. All solvents and reagents were commercially available and used as received unless stated otherwise. Pyrrole was distilled under N_2 and 1,3,5-tribromobenzene was purified by silica gel chromatography (eluted with hexanes). 5,10,15,20-Tetrakis(4-sulfonatophenyl)porphyrinatochloroiron(III), Fe(III)TPPS, was synthesized as previously reported.[1-3] THF, diethyl ether, and chloroform were dried using 3-Å molecular sieves. For the purification of **6**, an Isolera Prime Biotage fitted with a Sfär C18 column was employed. Analytical HPLC was performed on a Shimadzu Prominence-I LC-2030 Plus fitted with a Shimadzu Nexcol C18 5 μm column (50 × 3.0 mm). $CDCl_3$ was purchased from Cambridge Isotope Laboratories and used as received. ^1H, $^{13}C\{^1H\}$, and $^{29}Si\{^1H\}$ NMR spectra were recorded on a Bruker Avance III HD 500 NMR spectrometer equipped with a multinuclear Smart Probe. Signals in the ^1H, ^{13}C, and ^{29}Si NMR spectra are reported in ppm as chemical shifts from tetramethylsilane and were referenced using the $CHCl_3$ (^1H, 7.26 ppm) or HDO (^1H, 4.79 ppm) or $CDCl_3$ (^{13}C, 77.0 ppm) solvent signals or TMS in $CDCl_3$ (^{29}Si, 0.0 ppm). Deuterated phosphate-buffered saline (PBS-*d*) was obtained by lyophilizing an aliquot of proteo-PBS and redissolving the solid in an equivalent volume of D_2O. The following abbreviations were used to explain the multiplicities: s = singlet, d = doublet, t = triplet, q = quartet, m = multiplet. Glass background was removed from the ^{29}Si NMR spectra via backwards linear prediction of the first 100 points of the FID. UV-visible absorption spectra were measured on a Shimadzu UV-2401PC dual-beam spectrophotometer. IR spectra were recorded on a PerkinElmer Spectrum One FT-IR spectrometer. ESI mass spectra were obtained using a ThermoFisher LTQ Orbitrap Velos Pro. MALDI mass spectra were acquired using timsControl v 1.1.19 on a timsTOF fleX mass spectrometer (Bruker Scientific, Billerica,

MA) over the mass range 100−2000 Da. In positive reflectron mode, laser power was set to 12%, and laser application was set to MS Dried Droplet. Compounds were dissolved in DCM and 1 µl was mixed with 1 µl of matrix (50:50 α-cyano-4-hydroxycinnamic acid: 2,5-dihydroxybenzoic acid in a solution of 70:30 ACN: H_2O with 0.1% trifluoroacetic acid). Samples were spotted on a stainless steel MSP 96 spot target plate and allowed to air dry. For each compound, 1000 laser shots at 2000 Hz were delivered in a random walk across the spot. Data were subsequently analyzed in DataAnalysis v 5.3 (Bruker Scientific, Billerica, MA). Elemental analysis was performed by Midwest Microlabs (Indianapolis, IN) using an Exeter CE440 analyzer. Melting point data were collected using an electrothermal Mel-Temp apparatus with a Fluke 52 II thermocouple probe and temperatures are uncorrected. Solution phase magnetic moments were measured using a modified Evans method.[4]

Synthesis of (3,5-dibromophenyl)trimethylsilane (1).

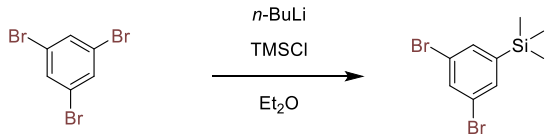

1

A previously reported procedure was modified.[5] 1,3,5-Tribromobenzene (13 g, 41.8 mmol) was dissolved in Et_2O (250 mL, 0.17 M) and sparged with N_2 for 10 min. This solution was cooled to –78 °C. *n*-BuLi (17.56 mL, 43.89 mmol) was added in a dropwise manner over 30 min using a syringe pump. The reaction was allowed to stir at –78 °C for an additional 30 min. Chlorotrimethylsilane (5.8 mL, 45.98 mmol) was added in a dropwise manner over 10 min. The solution was warmed to 0 °C over approximately 20 min. The 0 °C reaction mixture was filtered through a pad of silica, which was then washed with ether. The filtrates were combined and solvent was removed under reduced pressure to give crude (3,5-dibromophenyl)trimethylsilane as a yellow oil (12.457 g, 97% yield) that solidified upon standing at room temperature. This crude product was dissolved in hexanes and passed through a pad of silica. Solvent was removed from the eluent under reduced pressure to give an off-white solid (11.825 g 93% yield). Recrystallization from cold ethanol afforded the pure product as colorless needles (9.925 g, 78% yield). ^{1}H NMR (500 MHz, $CDCl_3$) δ 7.66-7.62 (m, 1H), 7.51 (s, 2H), 0.27 (s, 9H); $^{13}C\{^1H\}$ NMR (126 MHz, $CDCl_3$) δ 146.19, 134.62, 134.32, 123.34, –1.21; $^{29}Si\{^1H\}$ NMR (99 MHz, $CDCl_3$) δ –2.16; Melting point: 41.2 °C; Anal. Calcd for $C_9H_{12}Br_2Si$: C, 35.09; H, 3.93. Found: C, 34.61; H, 3.65.

Synthesis of 2,6-dibromo-4-trimethylsilylbenzaldehyde (2).

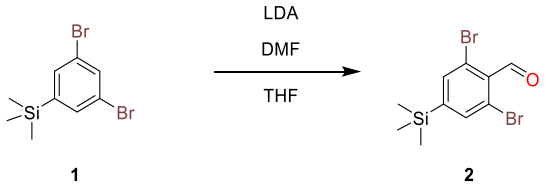

A procedure previously used to prepare aryl aldehydes was modified.[6] (3,5-Dibromophenyl)trimethylsilane (7 g, 22.9 mmol) was dissolved in THF (225 mL, 0.1 M), cooled to –78 °C, and sparged with N_2 for 10 min. Lithium diisopropylamide (2.0 M in THF/heptane/ethylbenzene, 45.8 mL, 91.8 mmol) was added in a dropwise manner over 30 min such that the reaction temperature, monitored with a thermocouple probe, did not exceed –75 °C. The reaction was stirred at this temperature for 1.5 h. DMF (7.9 mL, 103.28 mmol) was added in a dropwise manner and the reaction was stirred for an additional 1.5 h. Aqueous 1 M H_2SO_4 (100 mL) was added and the product was extracted with ether (100 mL). The organic layer was dried over sodium sulfate and filtered. The crude product was dry-loaded onto silica gel and purified by column chromatography (silica gel, hexanes:ether 95:5) yielding 2,6-dibromo-4-trimethylsilylbenzaldehyde as a pale-yellow oil that solidified while drying under vacuum (6.20 g, 80% yield). This crude product was then recrystallized from hot ethanol and the pale-yellow needles were collected by filtration. Two crops were collected (first crop 4.562 g, second crop 1.072 g, 73% combined yield). ^{1}H NMR (500 MHz, $CDCl_3$) δ 10.25 (s, 1H), 7.69 (s, 2H), 0.31 (s, 9H); $^{13}C\{^1H\}$ NMR (126 MHz, $CDCl_3$) δ 191.39, 150.50, 138.11, 132.71, 124.81, –1.41; Melting point: 89.8 °C; Anal. Calcd for $C_{10}H_{12}Br_2OSi$: C, 35.74; H, 3.60. Found: C, 35.28; H, 3.53.

Synthesis of 5,10,15,20-tetrakis(2,6-dibromo-4-(trimethylsilyl)phenyl)porphyrin (3).

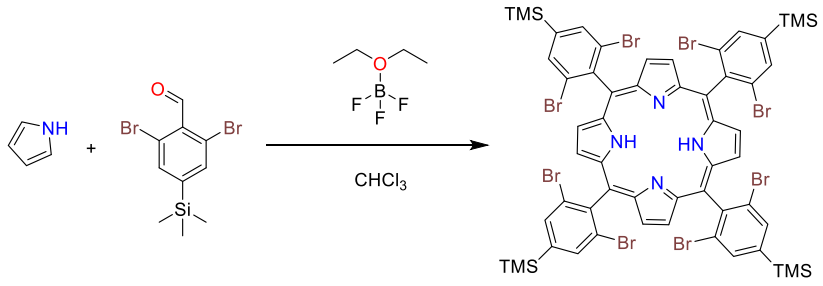

2 3

A procedure previously used to couple aldehydes and pyrrole into *meso*-substituted porphyrins was modified.[7] A mixture of 2,6-dibromo-4-trimethylsilylbenzaldehyde (1.754 g, 5.22 mmol), and pyrrole (350 mg, 5.22 mmol) in $CHCl_3$ (350 mL) and EtOH (0.2 mL) was added to a 1 L oven-dried round bottom flask fitted with a magnetic stirrer. The reaction mixture was sparged with N_2 for 20 min, followed by the addition of BF_3 etherate (185 mg, 1.3 mmol, 0.16 mL). The solution became yellow and slowly darkened to wine red. After stirring the solution for 16 h in the dark at room temperature, 2,3-dichloro-5,6-dicyano-1,4-benzoquinone (2.371 g, 10.4 mmol) was added in one portion, turning the solution black. This solution was allowed to stir for 2 h. The crude mixture was filtered through a pad of silica gel, which was then washed with chloroform. The combined filtrates yielded a purple solid after concentration under reduced pressure. This solid was washed with acetonitrile to give 5,10,15,20-tetrakis(2,6-dibromo-4-(trimethylsilyl)phenyl)porphyrin as a purple solid after drying (957 mg, 48% yield). X-ray quality crystals were grown by layering MeCN over the product in $CHCl_3$ to give purple plates. ^{1}H NMR (500 MHz, $CDCl_3$) δ 8.65 (s, 8H), 8.09 (s, 8H), 0.53 (s, 36H), –2.42 (s, 2H); $^{13}C\{^1H\}$ NMR (126 MHz, $CDCl_3$) δ 146.06, 142.97, 136.01, 128.76, 118.76, –0.89; Melting point: >400 °C; Anal. Calcd for $C_{56}H_{54}Br_8N_4Si_4$: C, 43.83; H, 3.55; N, 3.65. Found: C, 43.36; H, 3.52; N, 3.60; UV/Vis ($CHCl_3$) λ_{abs} (log ε): 406 (sh), 424 (4.64), 518 (3.35), 593 (2.86).

Synthesis of 5,10,15,20-tetrakis(2,6-diphenyl-4-(trimethylsilyl)phenyl)porphyrin (4).

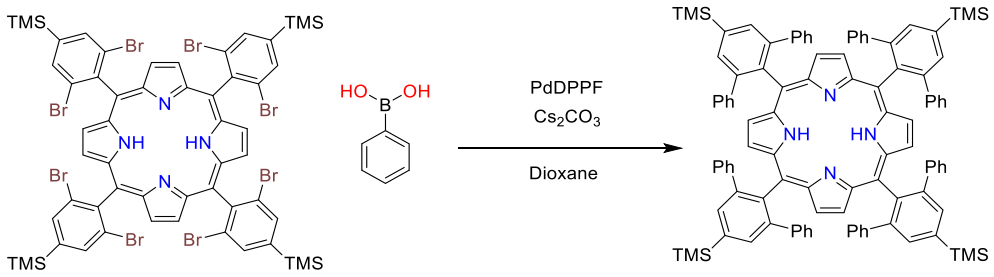

3 **4**

5,10,15,20-Tetrakis(2,6-dibromo-4-(trimethylsilyl)phenyl)porphyrin (300 mg, 0.1967 mmol), [1,1′-bis(diphenylphosphino)ferrocene]dichloropalladium(II) (144 mg, 0.1967 mmol), phenylboronic acid (576 mg, 4.7213 mmol), and cesium carbonate (2.061 g, 6.251 mmol) were dissolved in a mixture of dioxane (20 mL) and H_2O (1 mL). The solution was sparged with N_2 for 5 min. The reaction was sealed with a septum and stirred at 100 °C for 14 h. The crude reaction mixture was stripped of solvent under reduced pressure. The residue was taken up in chloroform (50 mL) and passed through a pad of silica gel. The filtrate was dried to give a purple solid that was washed with acetonitrile. The washed solid was dissolved in chloroform and dry loaded onto silica gel. The product was purified by column chromatography (silica, hexanes:chloroform 1:1). The eluted product was concentrated to give **4** as a purple solid (256 mg, 86% yield). X-ray quality crystals were grown by layering MeCN over the product in $CHCl_3$ to give purple plates. ^{1}H NMR (500 MHz, $CDCl_3$) δ 8.38 (s, 8H), 7.77 (s, 8H), 6.56 (d, J = 7.7 Hz, 16H), 6.40 (t, J = 7.2 Hz, 8H), 6.22 (t, J = 7.4 Hz, 16H), 0.51 (s, 36H), –3.40 (s, 2H); ^{13}C{^{1}H} NMR (126 MHz, $CDCl_3$) δ 144.80, 142.44, 140.75, 139.39, 133.66, 129.44, 126.67, 125.22, 116.12, –0.62; ^{29}Si{^{1}H} NMR (99 MHz, $CDCl_3$) δ –3.44; Melting point: >400 °C; HRMS (MALDI) *m/z*: $[M+H]^+$ Calcd for $C_{104}H_{95}N_4Si_4^+$ 1512.6662; Found 1512.6650; UV/Vis ($CHCl_3$) λ_{abs} (log ε): 419 (sh), 439 (4.54), 495 (2.62), 533 (3.17), 570 (2.93), 610 (2.79), 670 nm (2.34).

Synthesis of 5,10,15,20-tetrakis(2,6-diphenyl-4-(trimethylsilyl)phenyl)porphyrinatohydroxoiron(III) (5).

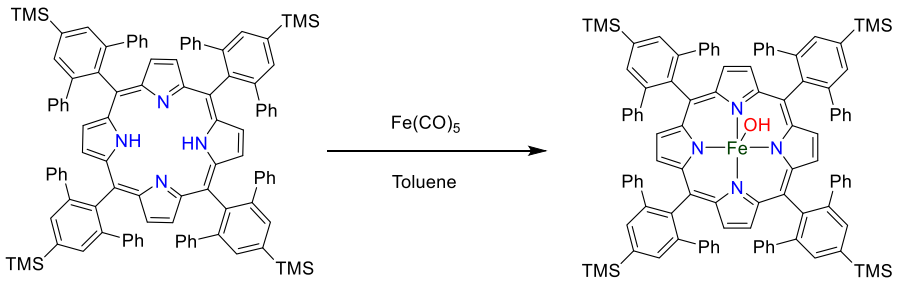

4 5

A procedure previously used for inserting iron into sterically hindered porphyrins was modified.[8] 5,10,15,20-Tetrakis(2,6-diphenyl-4-(trimethylsilyl)phenyl)porphyrin (200 mg, 0.1325 mmol), iron pentacarbonyl (2.589 g, 13.2 mmol, 1.786 mL), and iodine (101 mg, 0.397 mmol) were dissolved in toluene (30 mL) and refluxed for 5 h under N_2. This solution was then refluxed another 1 h under ambient conditions. The solution was concentrated under reduced pressure. The residue was taken up in $CHCl_3$ and filtered through a pad of Celite. The filtrate was added to a separatory funnel and washed with 1 M $NaOH_{(aq)}$. The organic layer was dried with anhydrous sodium sulfate, filtered, and concentrated under reduced pressure to give **5** as a green solid (183 mg, 88% yield). X-ray quality dark purple plates were grown by layering MeCN over a solution of the product in $CHCl_3$. ^{1}H NMR (500 MHz, $CDCl_3$; paramagnetic) δ 82.16 (β-pyrrole); Melting point: >400 °C; HRMS (MALDI) *m/z*: $[M–OH]^+$ Calcd for $C_{104}H_{92}FeN_4Si_4^+$ 1565.5777; Found 1565.5786. $[M+H]^+$ Calcd for $C_{104}H_{94}FeN_4OSi_4^+$ 1583.5883; Found 1583.5887; UV/Vis ($CHCl_3$) λ_{abs} (log ε): 360 (sh), 379 (4.52), 443 (5.14), 524 (4.07), 596 (sh); μ_{eff} (Evans', $CDCl_3$): 5.49 μ_B; Anal. Calcd for $C_{104}H_{93}FeN_4OSi_4 \cdot CH_2Cl_2 \cdot C_2H_3N$: C, 75.20; H, 5.78; N, 4.10. Found: C, 74.95; H, 5.70; N, 3.97, Solvents added to the calculated elemental analysis are corroborated by the diffraction data. See below.

Synthesis of Sodium 5,10,15,20-tetrakis(2,6-diphenyl-4-(sulfonate)phenyl)porphyrinatohydroxoiron(III) (6).

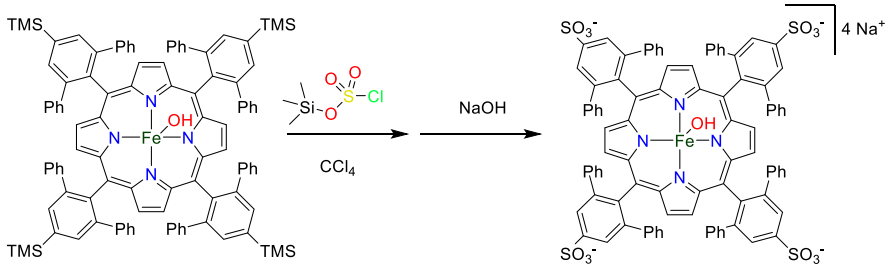

5 6

A procedure previously used to convert aryl TMS groups into chlorosulfonates was modified.[9] Compound **5** (50 mg, 0.0316 mmol) was dissolved in CCl_4 (4 mL). To this solution was added trimethylsilyl chlorosulfonate (72 mg, 0.38 mmol, 0.058 mL). The solution was stirred at reflux for 60 min under N_2. After cooling to room temperature, 1 M $NaOH_{(aq)}$ (5 mL) was added and the reaction was stirred vigorously for 10 min. This solution was diluted with DI water (50 mL), washed with chloroform (50 mL), and stripped of solvent under reduced pressure. The resulting green solid was dry-loaded onto C18-functionalized silica gel and eluted across 25 g of stationary phase (6.35 cm) with a gradient of H_2O/MeCN containing 0.01% TFA (5-95% MeCN over 15 min). The first colored fraction was collected and dialyzed against DI water for 3 d (changing dialysate every 12 h). The retentate was lyophilized yielding the tetrasodium salt **6** as a dark purple/black solid (22 mg 40% yield). Weakly diffracting crystals of **6** were grown from $CHCl_3$/DMSO. Higher-quality crystals (**6**$_{DMSO}$) were grown slowly by layering $CHCl_3$ over the product in DMSO. ^{1}H NMR (500 MHz, PBS-*d*, 10% ^{t}BuOH; paramagnetic) δ 78.65 (β-pyrrole); HRMS (ESI) *m/z*: $[M–4Na–OH+H]^{3–}$ Calcd for $C_{92}H_{57}FeN_4O_{12}S_4^{3–}$ 531.0740; Found 531.0711. $[M–3Na–OH+H]^{2–}$ Calcd for $C_{92}H_{57}FeN_4NaO_{12}S_4^{2–}$ 808.1057; Found 808.1004. $[M–4Na–OH+H+MeOH]^{3–}$ Calcd for $C_{93}H_{61}FeN_4O_{13}S_4^{3–}$ 541.7494; Found 541.7454. $[M–OH–4Na]^{4–}$ Calcd for $C_{92}H_{56}FeN_4O_{12}S_4^{4–}$ 398.3046; Found 398.3028; HPLC (H_2O/MeCN): t_r = 1.10 min; UV/Vis (PBS) λ_{abs} (log ε): 333 (3.19), 431 (3.82), 509 (sh), 545 (sh); μ_{eff} (Evans', PBS-*d*): 5.22 μ_B

***In situ* reduction of 6.**

For NMR spectroscopic characterization, compound **6** (6 mg) was dissolved in PBS-*d* (1.5 mL) containing 10% ^{t}BuOH. The alcohol was included for the Evans' Method μ_{eff} determination. The alcohol also increases the solubility of the compound allowing highly concentrated solutions to be used to compensate for the decrease in the signal-to-noise ratio from paramagnetic broadening. Attempts to run the NMR reaction at equivalent concentrations in the absence of the ^{t}BuOH resulted in precipitation over the course of minutes. The same situation held for the following reaction with CO. Note that the UV-vis experiments (*vide infra*), which are performed at lower concentrations, confirm that this and the subsequent reaction proceed without the added ^{t}BuOH. The solution was sparged with N_2 for 5 min and an ^{1}H NMR spectrum was acquired (Figure S13). Sodium dithionite (1 mg) was added and an ^{1}H NMR spectrum was acquired (Figure S14). ^{1}H NMR (500 MHz, PBS-*d*, 10% ^{t}BuOH; paramagnetic) δ –3.63 (β-pyrrole)[10]; μ_{eff} (Evans', PBS-*d*, 10% ^{t}BuOH): 3.69 μ_B

For UV-vis characterization, compound **6** was dissolved in PBS and diluted to 0.02 mM. A minimal amount of sodium dithionite was added to effect reduction of **6**, which resulted in an immediate change in the electronic absorption spectrum. UV/Vis (PBS) λ_{abs} (log ε): 448 (5.08), 551 (3.81), 578 (sh), 625 (3.38). Air was bubbled through the solution to remove any excess sodium dithionite as assessed by reduction in intensity of the absorption at 315 nm. Once all of the dithionite had been consumed, the quiescent solution was left open to air and electronic absorption spectra were acquired at 90 s intervals (Figure S17).

***In situ* formation of 7.**

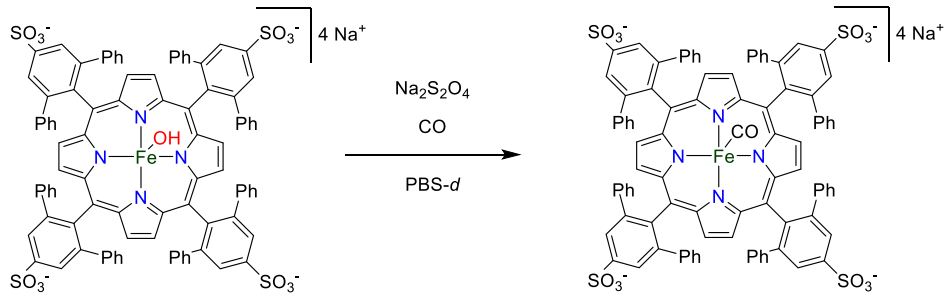

6 **7**

For NMR spectroscopic characterization, compound **6** (6 mg) was dissolved in PBS-*d* containing 10% ^{t}BuOH (1.5 mL). The solution was sparged with N_2 for 5 min and sodium dithionite (1 mg) was added to the NMR tube. Then, CO was bubbled through the solution for approximately 5 s. The NMR tube was sealed and an ^{1}H NMR spectrum was acquired (Figure S15). ^{1}H NMR (500 MHz, PBS-*d*, 10% ^{t}BuOH) δ 8.09 (s, 8H), 7.98 (s, 8H), 6.35 (d, J = 7.2 Hz, 16H), 6.01 (s, 8H), 5.95-5.87 (m, 16H); μ_{eff} (Evans', PBS-*d*, 10% ^{t}BuOH): 0 μ_B;

For UV-vis characterization, compound **6** was dissolved in PBS and diluted to 0.02 mM. A minimal amount of sodium dithionite was added to effect reduction of **6**. CO was bubbled through for 5 s to generate compound **7**, which resulted in an immediate change in the electronic absorption spectrum. UV/Vis (PBS) λ_{abs} (log ε): 444 (5.08), 557 (3.85), 624 (3.48). Air was bubbled through the solution to remove any excess sodium dithionite as assessed by reduction in intensity of the absorption at 315 nm. Once all of the dithionite had been consumed, the quiescent solution was left open to air and electronic absorption spectra were acquired at 600 s intervals (Figure S18).

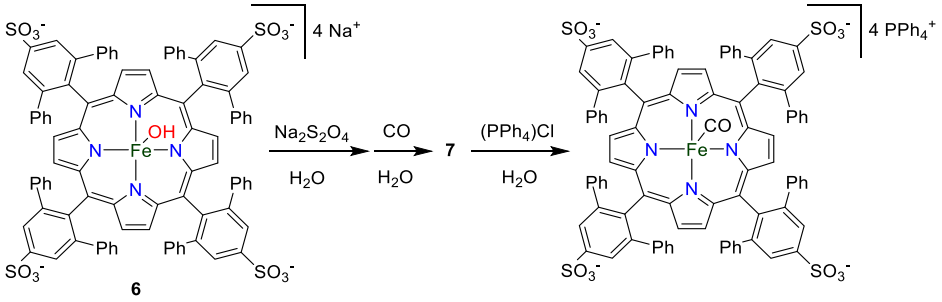

To collect IR data, compound **6** (5 mg) was dissolved in DI water (5 mL). The solution was sparged with nitrogen and excess sodium dithionite was added (1 mg). CO was bubbled through the solution for 5 s. To this solution was added an excess of tetraphenylphosphonium chloride (5 mg). The resulting precipitate was collected, washed with DI water, and dried under a stream of N_2 for 5 min. The resulting solid was used to prepare a KBr pellet for IR spectroscopic measurement (Figure S19).

X-ray crystallography. Crystals of **4**·2MeCN, **5**·DCM·MeCN, **6**, and **6**$_{DMSO}$·4DCM were grown as described above, selected under a microscope, loaded onto a nylon fiber loop using Paratone-N, and mounted onto a Rigaku XtaLAB Synergy-S single-crystal diffractometer. Each crystal was cooled to 100 K under a stream of nitrogen. Diffraction of Cu Kα radiation from a PhotonJet-S microfocus source was detected using a HyPix-6000HE hybrid photon counting detector. Screening, indexing, data collection, and data processing were performed with CrysAlis^{Pro}.[11] The structures were solved using SHELXT and refined using SHELXL as implemented in OLEX2 following established strategies.[12-15] The contents of the unit cell of **4**·2MeCN are depicted in Figure S20. The contents of the unit cell of **5**·DCM·MeCN are depicted in Figure S21. The crystals of **6** were twinned and diffracted weakly. The diffraction data allowed the proposed connectivity of the iron complexe to be confirmed (Figure S22), but were not suitable for detailed analysis of bond metrics. Notably, in **6**, the apical ligand is located 1.9 Å from the Fe center and exhibited an

electron density consistent with an O atom. For the atomic-resolution crystal structures of **4**·2MeCN, **5**·DCM·MeCN, and $\mathbf{6}_{\mathbf{DMSO}}$·4DCM, all non-H atoms were refined anisotropically and carbon-bound H atoms were placed at calculated positions and refined with a riding model and coupled isotropic displacement parameters (1.2 × U_{eq} for aryl groups and 1.5 × U_{eq} for methyl groups). For **5**·DCM·MeCN, the oxygen-bound H atom was placed at a calculated position and refined using a riding model that additionally allowed refinement of the torsional setting of the H and the O–H bond length, the latter restrained to 0.84(2) Å. Refinement parameters for **4**·2MeCN, **5**·DCM·MeCN, and $\mathbf{6}_{\mathbf{DMSO}}$·4DCM are collected in Table S1. The unit cell parameters for **6** are collected in Table S2.

CO abstraction from COHb. A stock solution of COHb was created by dissolving bovine Hb (5 mg) in 1 mL of PBS containing 5.7 mM sodium dithionite that had been sparged with N_2. CO was bubbled through this solution for 5 s. N_2 was slowly bubbled through this solution for 20 min to remove excess CO. Working solutions were prepared from this stock by dilution with PBS containing 5.7 mM sodium dithionite. Concentrations were determined with the mass of Hb used to prepare the stock solution and a molecular weight of 64,500 g/mol. For CO abstraction, a 2.5 μM PBS solution of COHb was prepared and titrated with a PBS solution of **6** or Fe(III)TPPS. Equivalents of **6** and Fe(III)TPPS were calculated per heme unit of Hb (i.e., 4 × molar quantity of protein). Spectra are presented in Figures 3C and S24.

Reduced 6 protects Hb from CO. A stock solution of bovine hemoglobin was prepared by dissolving 5 mg in 1 mL of N_2-sparged PBS containing 5.7 mM sodium dithionite. Working solutions were prepared from this stock by dilution with PBS containing 5.7 mM sodium

dithionite. Concentrations were determined with the mass of Hb used to prepare the stock solution and a molecular weight of 64,500 g/mol. From this stock, a working solution containing 2.5 μM Hb and 10 μM reduced **6** (prepared from *in situ* reduction of **6**) was prepared and titrated with CO-saturated water (approx. 1 mM $CO_{(aq)}$). UV-vis spectra were acquired after addition of 1 and 2 equivalents (with respect to **6**) of CO (Figure S23).

Hemolytic potential of reduced 6. Defibrinated bovine blood (Hemostat Laboratories) was diluted with PBS containing 5.7 mM sodium dithionite. This mixture was centrifuged for 30 s at 760 × g. The supernatant was discarded, and the pellet was washed with PBS containing 5.7 mM sodium dithionite. The pellet was suspended in PBS containing 5.7 mM sodium dithionite to give a suspension with A_{700} = 1.0. An aliquot of this suspension was lysed and the absorbance at 420 nm was used to quantify the amount of COHb ($\varepsilon = 10^{5.63}$). Based on this concentration, 1 equiv of compound **6**, which was reduced immediately, was added to the suspension of cells. After the addition, turbidity was monitored continuously at 700 nm. This process was repeated both in the absence of any added species (negative control) and upon addition of a RBC-lysing solution (1.5 M NH_4Cl) (Figure S25).

CO abstraction from CO-treated RBCs. Defibrinated bovine blood (Hemostat Laboratories) was diluted with PBS containing 5.7 mM sodium dithionite. CO was bubbled through this suspension for 5 s. This mixture was centrifuged for 30 s at 760 × g. The supernatant was discarded, and the pellet was washed with PBS containing 5.7 mM sodium dithionite. This washing was repeated three more times to remove excess CO. An aliquot of the stock suspension of CO-treated RBCs was added to a quartz cuvette containing 1 mL of DI water to lyse the cells. The

concentration of COHb was assessed by measuring the absorbance at 420 nm ($\varepsilon = 10^{5.63}$) of this lysate. For abstraction studies, an aliquot of the stock suspension of CO-treated RBCs was diluted to 1 mL with PBS containing 5.7 mM sodium dithionite. Compound **6**, which is reduced *in situ*, was added in increments based on the concentration of COHb determined in the lysate. A UV-vis spectrum was acquired after each addition (Figure 4).

Time-course CO removal from CO-treated RBCs. Defibrinated bovine blood (Hemostat Laboratories) was diluted with PBS containing 5.7 mM sodium dithionite. CO was bubbled through this suspension for 5 s. This mixture was centrifuged for 30 s at 760 × g. The supernatant was discarded, and the pellet was washed with PBS containing 5.7 mM sodium dithionite. This washing was repeated three more times to remove excess CO. An aliquot of the stock suspension of CO-treated RBCs was added to a quartz cuvette containing 1 mL of DI water to lyse the cells. The concentration of COHb was assessed by measuring the absorbance at 420 nm ($\varepsilon = 10^{5.63}$) of this lysate. For time-course CO removal, an aliquot of the stock suspension of CO-treated RBCs was diluted to 1 mL with PBS containing 5.7 mM sodium dithionite. A full equivalent of compound **6** (which is reduced *in situ*) was added, the suspension was rapidly mixed, and absorbance at 420 nm was monitored continuously (Figure S26).

Table S1. Refinement Details for High-Resolution Crystal Structures

Compound	**4**·2MeCN	**5**·DCM·MeCN	**6**$_{\mathbf{DMSO}}$·4DCM
Formula	$C_{108}H_{100}N_6Si_4$	$C_{107}H_{98}Cl_2FeN_5OSi_4$	$C_{111}H_{99}Cl_{21}FeN_4Na_3O_{18}S_{10}$
FW	1594.29	1709.01	2966.81
T (K)	100.0(1)	100.0(1)	100.0(1)
λ (Å)	1.54184	1.54184	1.54184
Crystal System	Triclinic	Monoclinic	Triclinic
Space group	$P\bar{1}$	$P2_1/c$	$P\bar{1}$
a (Å)	13.1696(2)	16.3187(2)	14.03520(10)
b (Å)	13.5821(2)	12.8480(2)	14.48810(10)
c (Å)	16.0892(2)	23.5087(2)	16.95090(10)
α (°)	89.2370(10)		72.6450(10)
β (°)	71.1150(10)	106.80000(10)	80.2710(10)
γ (°)	61.112(2)		88.616(2)
Volume (Å^3)	2348.33	4718.53(10)	86.7770(10)
Z	1	2	1
ρ_{calc} (Mg/m^3)	1.127	1.203	1.519
Size (mm^3)	0.25×0.19×0.05	0.31×0.17×0.05	0.15×0.08×0.08
θ range (°)	2.95-67.07	2.79-76.74	2.77-67.08
Total data	89543	67527	95102
Unique data	8389	8417	11584
Parameters	540	588	831
Completeness (%)	100	99.9	99.9
R_{int} (%)	4.46	3.59	3.48
R_1 (%, I > 2σ)	3.38	6.48	5.73
R_1 (%, all data)	3.57	6.90	5.90
wR_2 (%, I > 2σ)	8.59	18.16	15.81
wR_2 (%, all data)	8.72	18.47	15.95
S	1.041	1.065	1.037

Table S2. Crystallographic Parameters for Low-Resolution Crystal Structure of **6**

Compound	**6**
T (K)	100.0(1)
λ (Å)	1.54184
Crystal System	Tetragonal
Space group	$P4_2/n$
a (Å)	23.1879(2)
c (Å)	24.2311(3)
Volume (Å^3)	13028.5(2)
Z	4

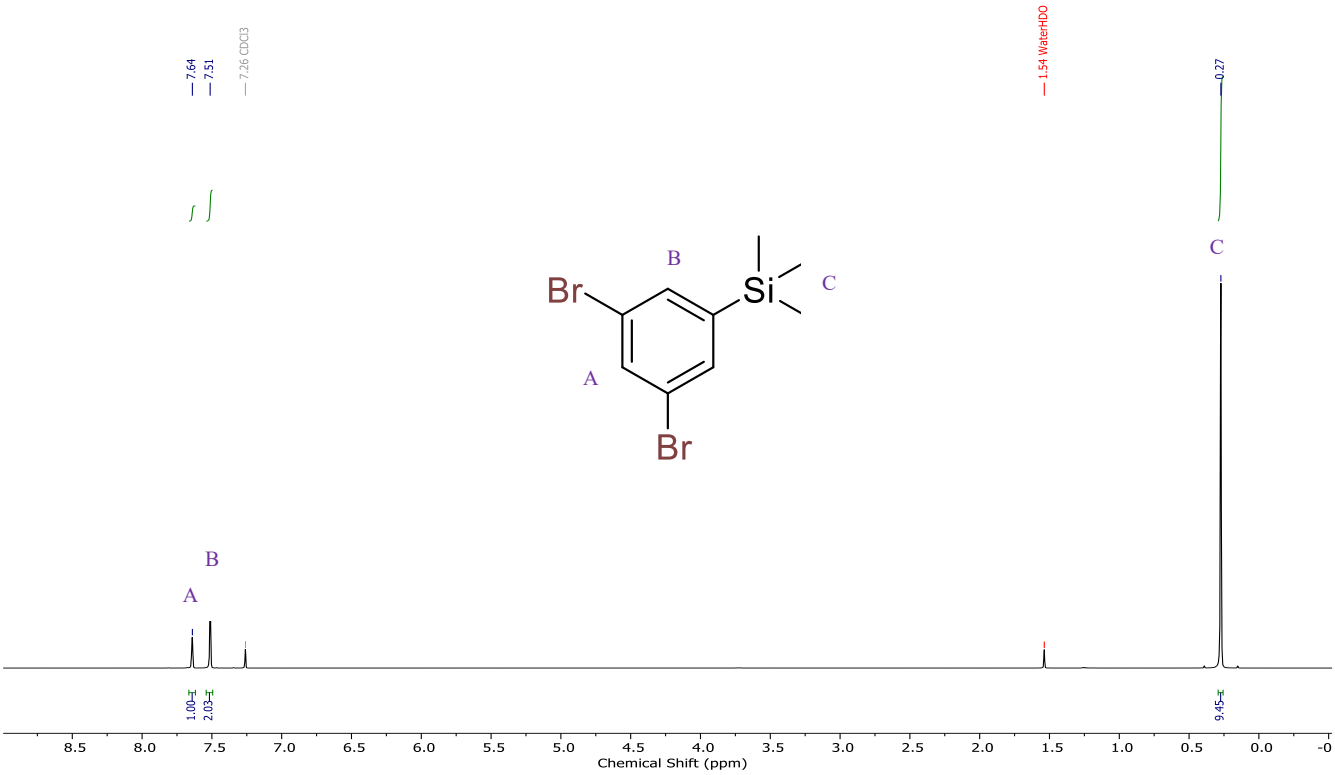

Figure S1. ^{1}H NMR spectrum (500 MHz, $CDCl_3$) of **1**.

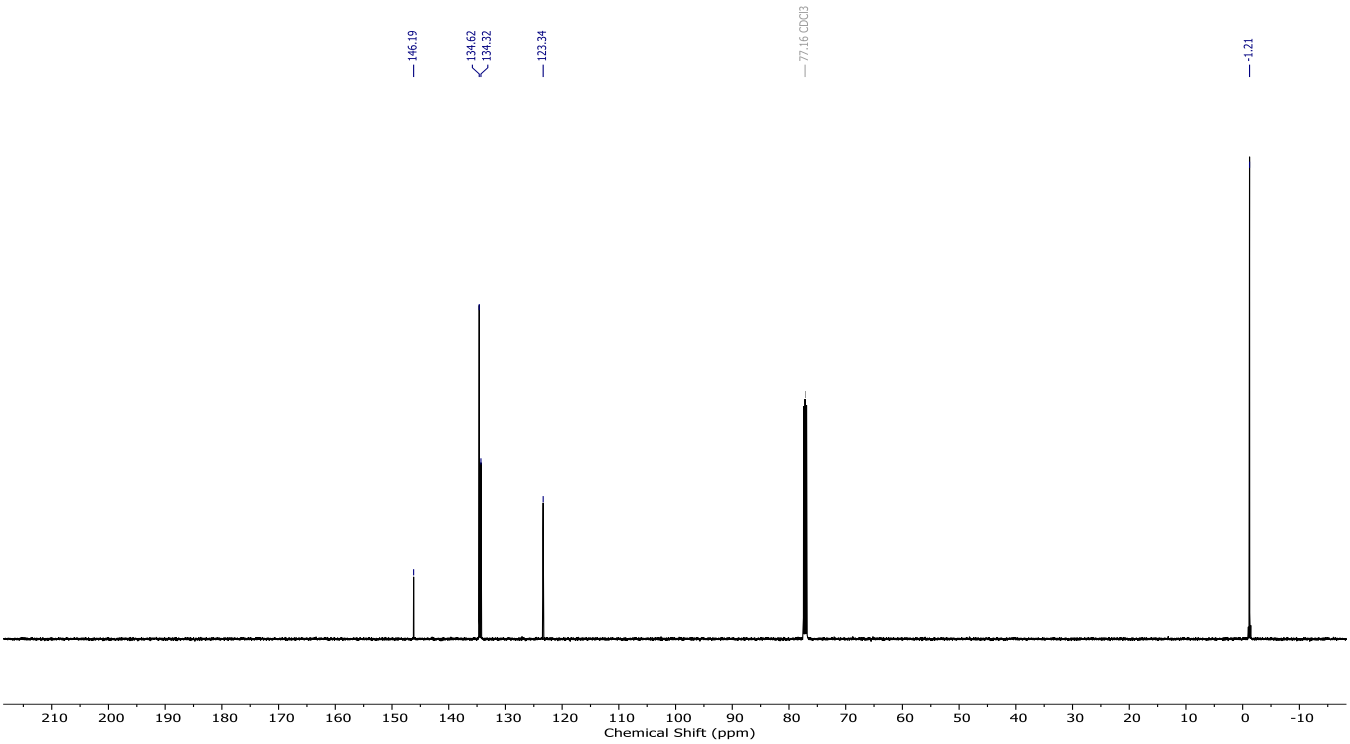

Figure S2. $^{13}C\{^{1}H\}$ NMR spectrum (126 MHz, $CDCl_3$) of **1**.

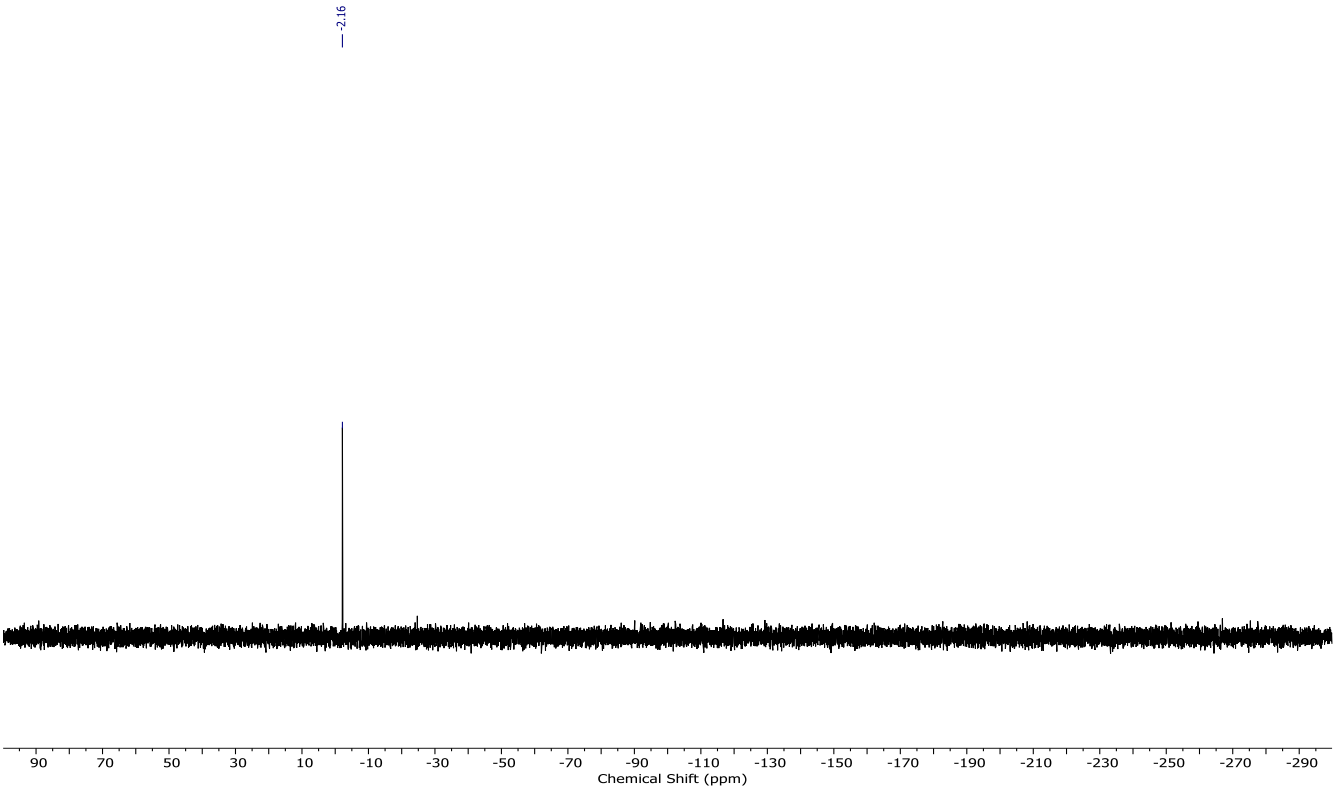

Figure S3. $^{29}Si\{^{1}H\}$ NMR spectrum (99 MHz, $CDCl_3$) of **1**.

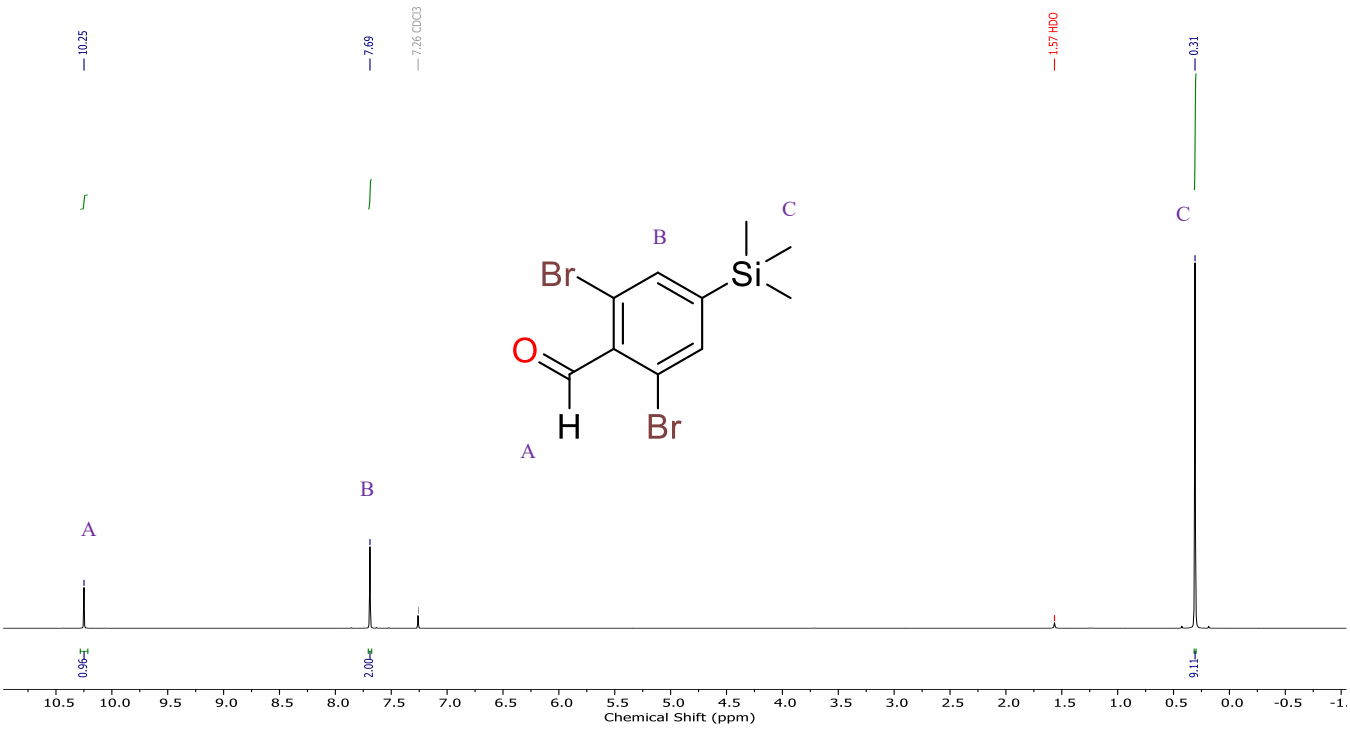

Figure S4. ^{1}H NMR spectrum (500 MHz, $CDCl_3$) of **2**.

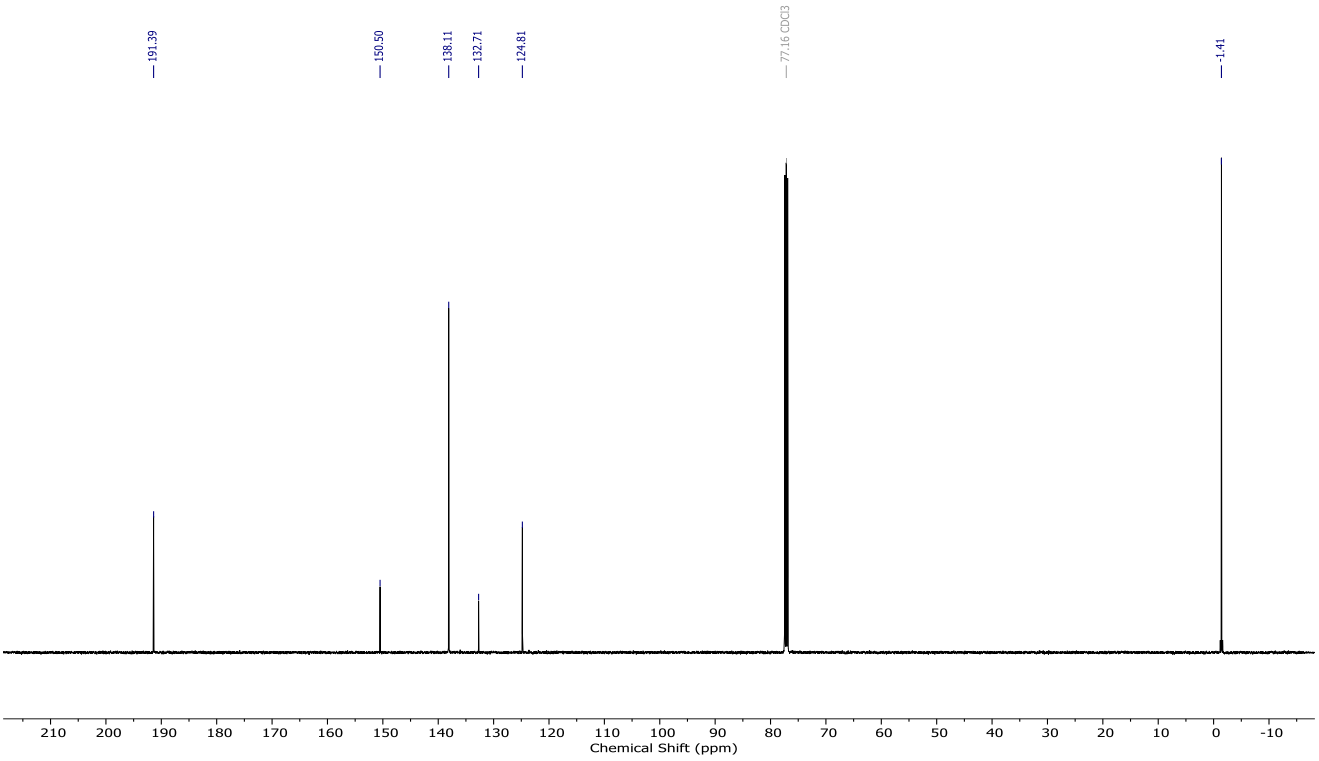

Figure S5. $^{13}C\{^{1}H\}$ NMR spectrum (126 MHz, $CDCl_3$) of **2**.

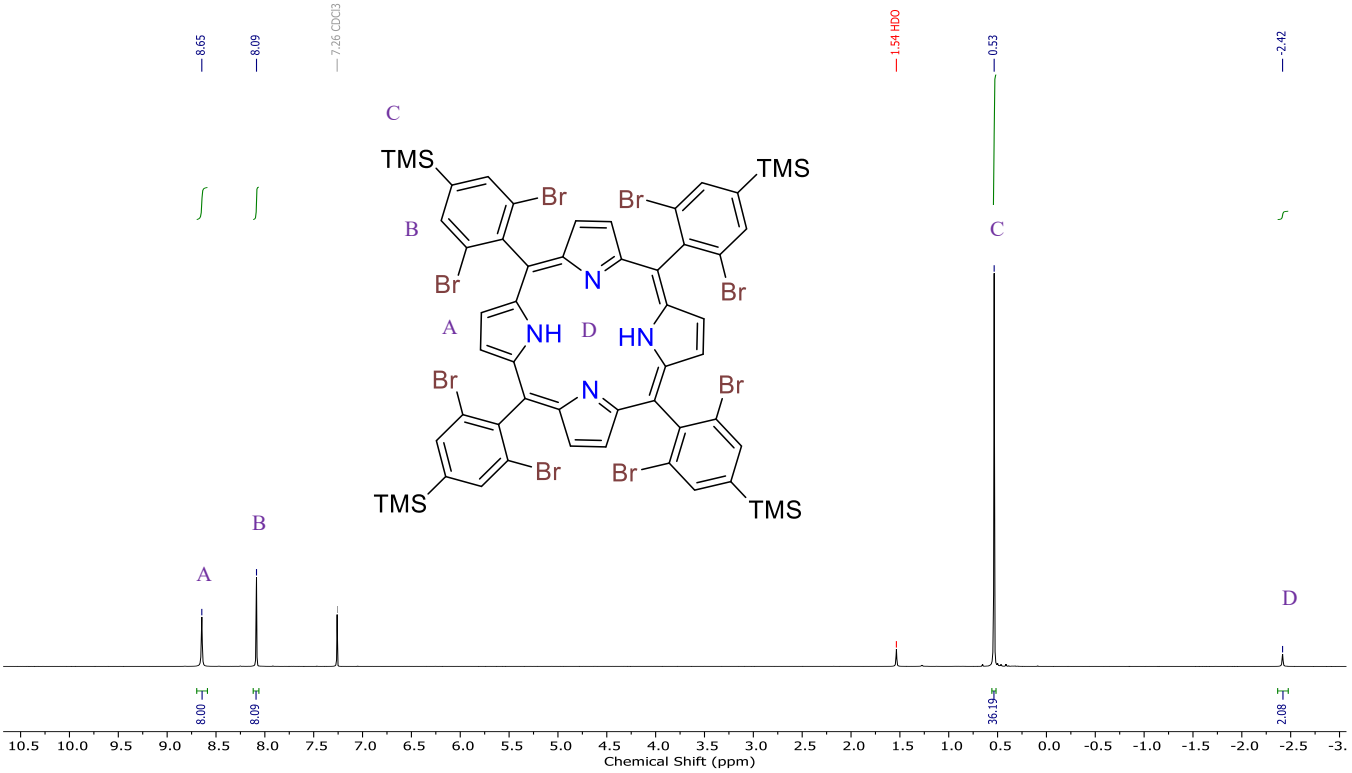

Figure S6. ^{1}H NMR spectrum (500 MHz, $CDCl_3$) of **3**.

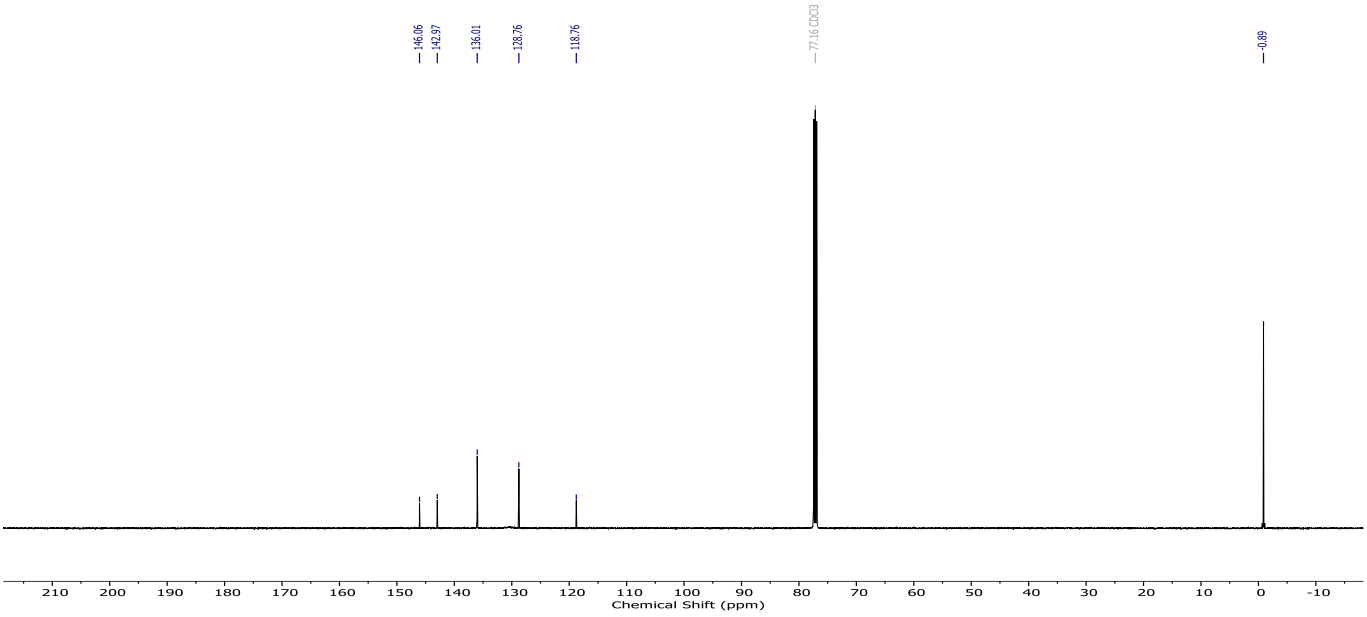

Figure S7. ^{13}C{^{1}H} NMR spectrum (126 MHz, $CDCl_3$) of **3**.

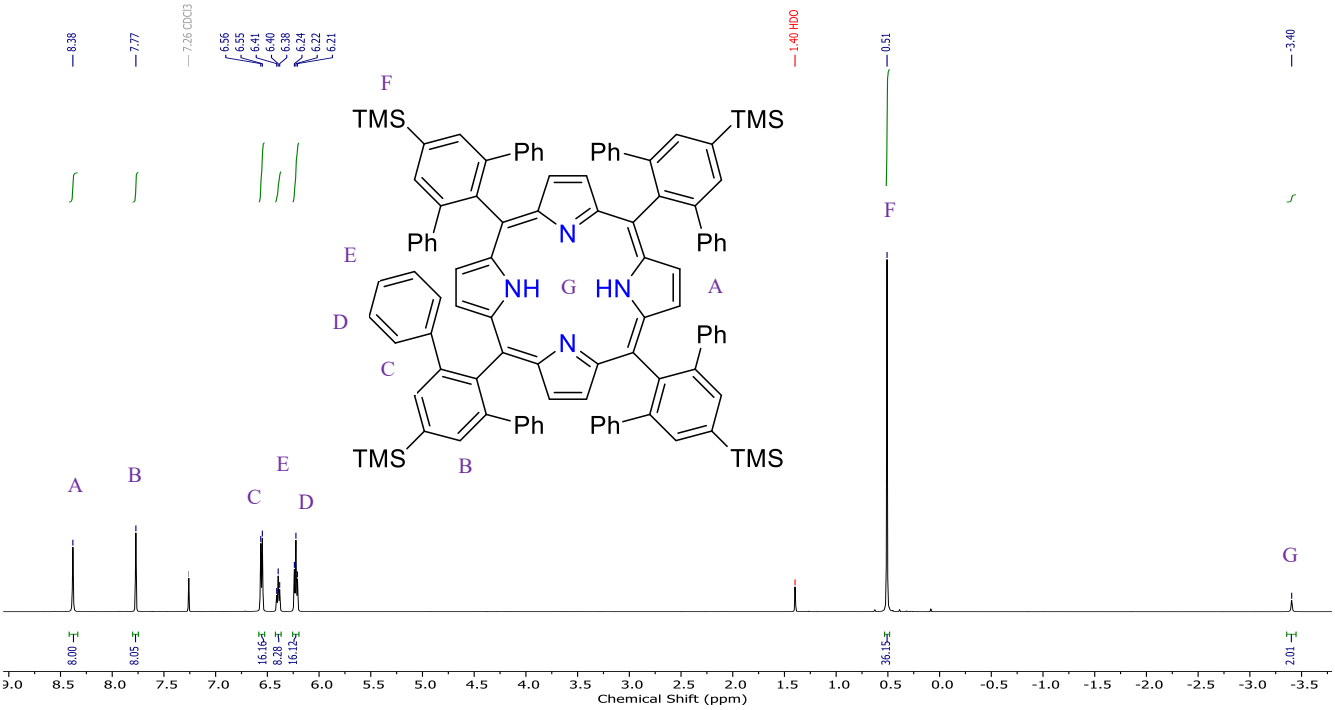

Figure S8. ^{1}H NMR spectrum (500 MHz, $CDCl_3$) of **4.**

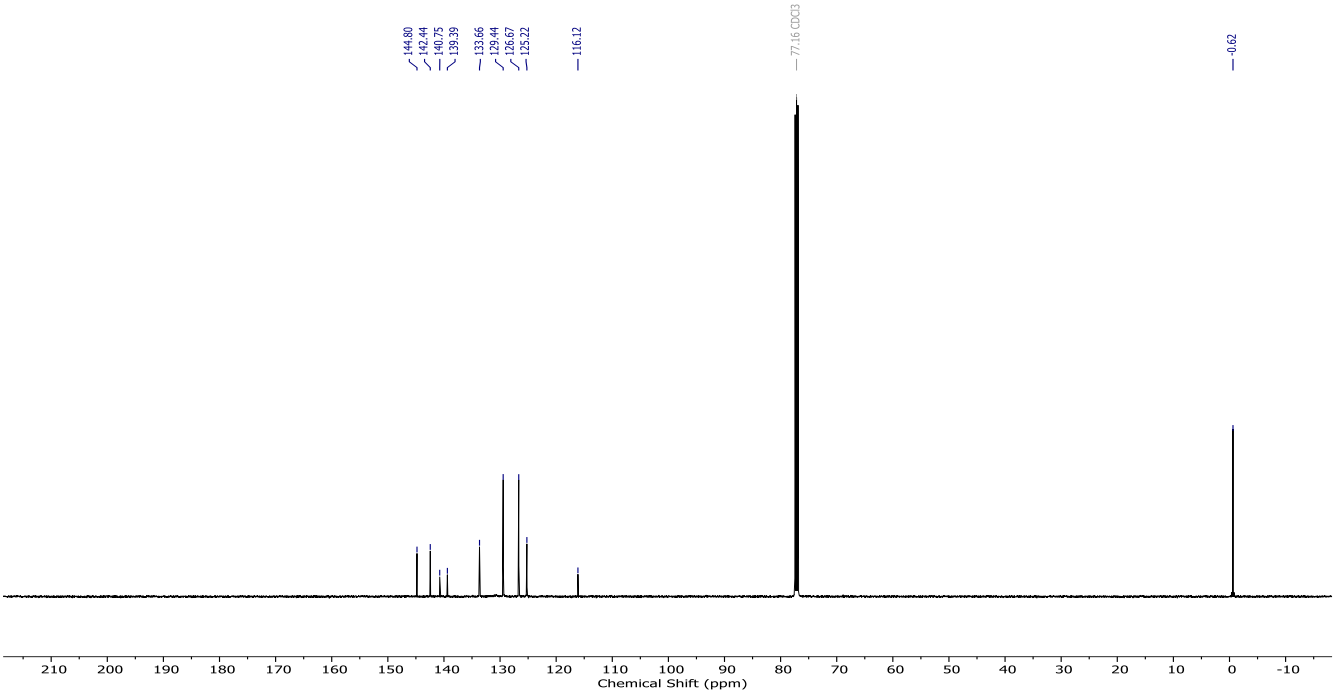

Figure S9. $^{13}C\{^{1}H\}$ NMR spectrum (126 MHz, $CDCl_3$) of **4.**

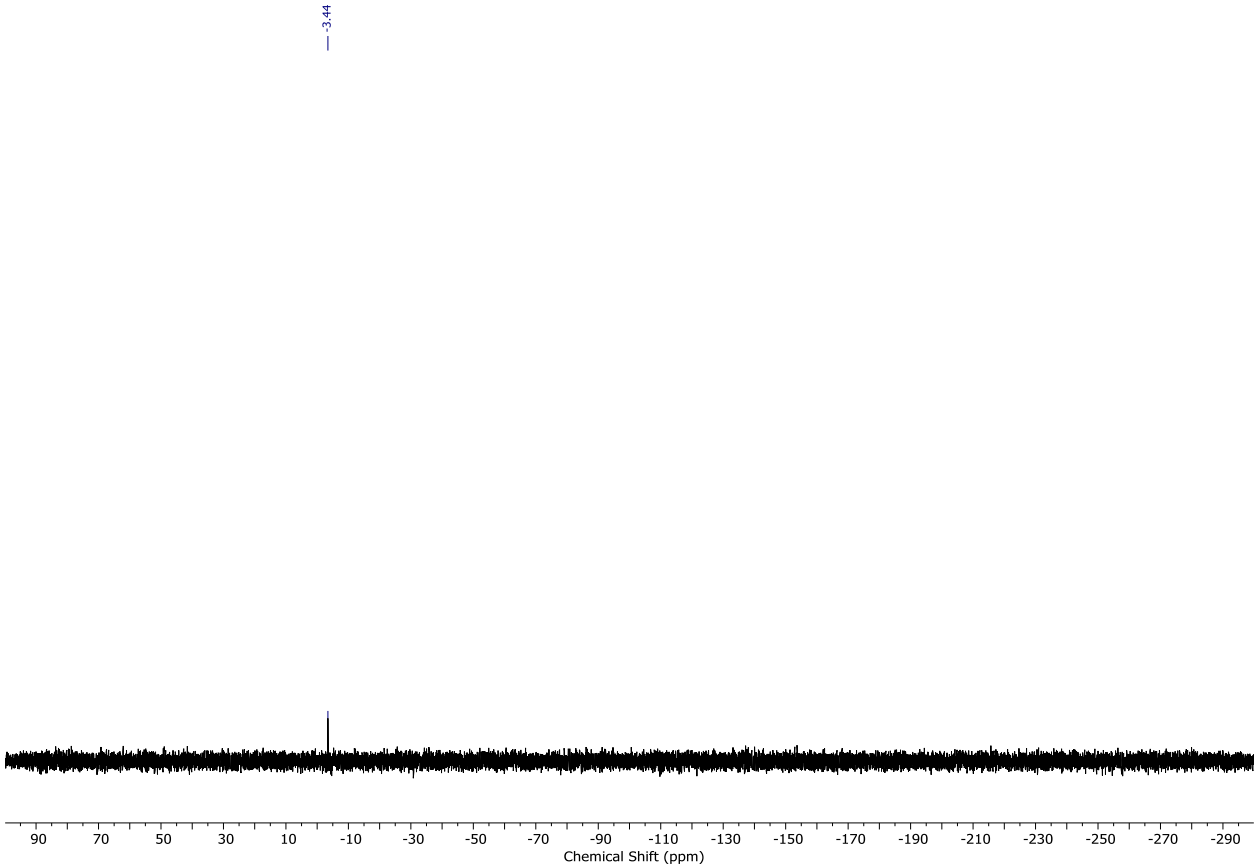

Figure S10. $^{29}Si\{^{1}H\}$ NMR spectrum (99 MHz, $CDCl_3$) of **4.**

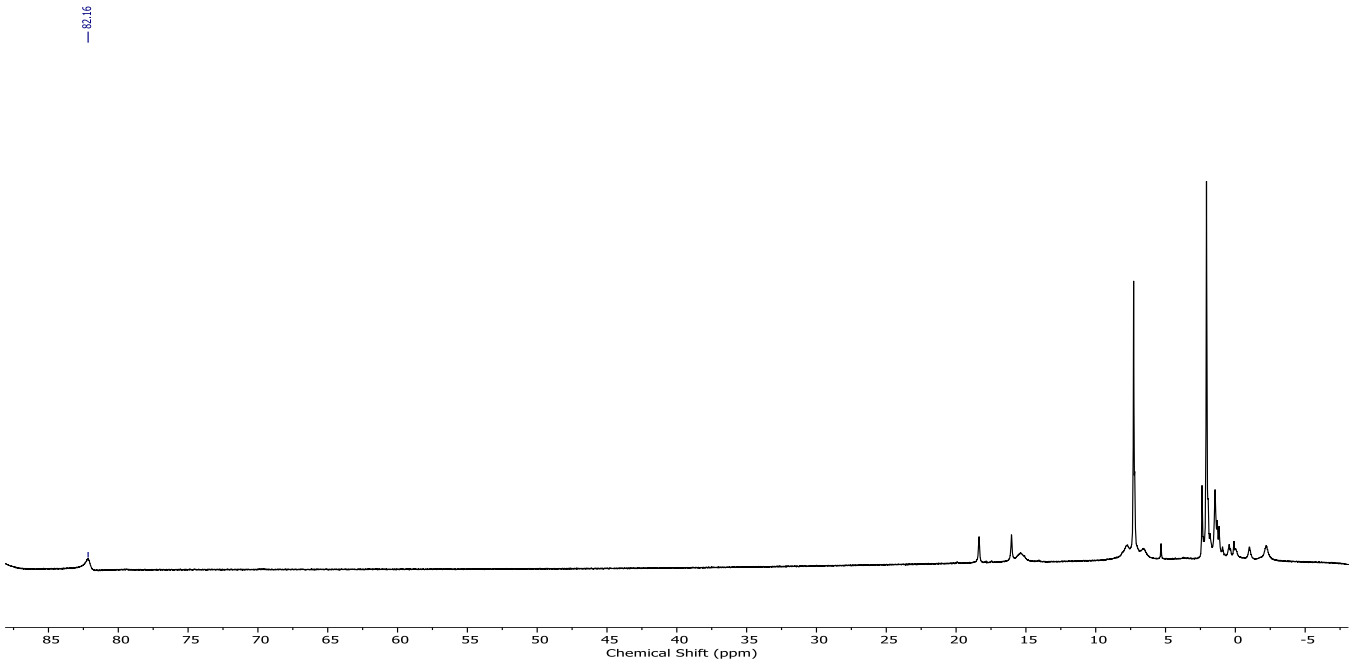

Figure S11. ^{1}H NMR spectrum (500 MHz, $CDCl_3$) of **5**. NB: this substance is paramagnetic.

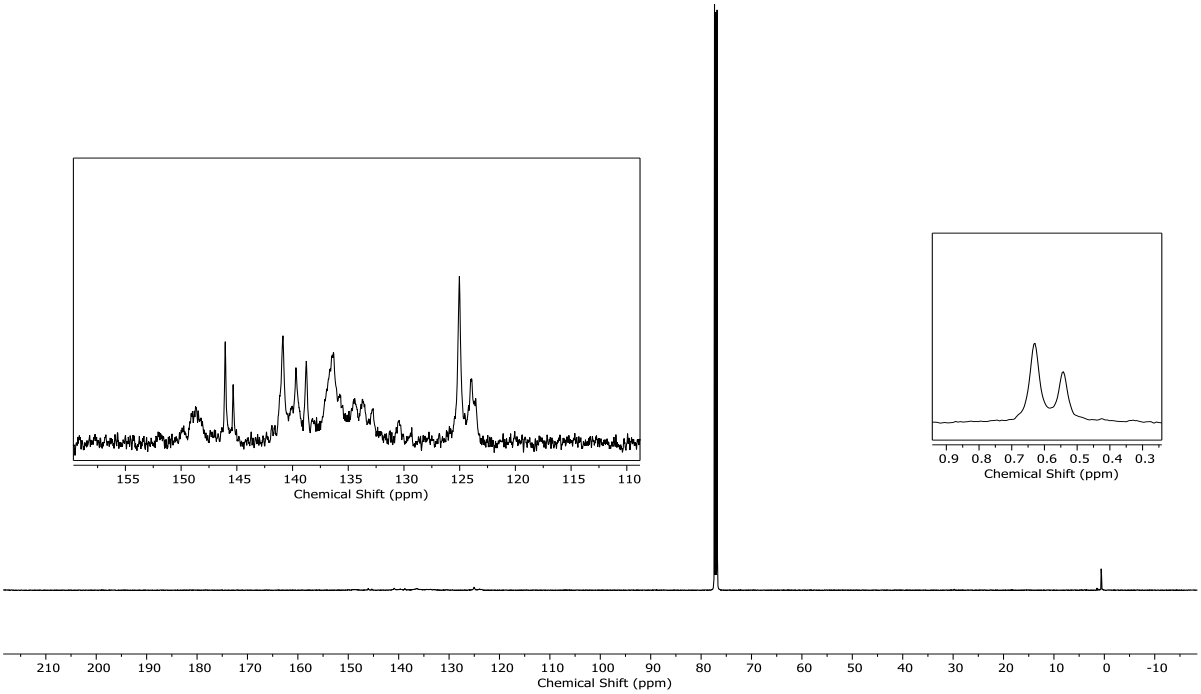

Figure S12. ^{13}C NMR spectrum (500 MHz, $CDCl_3$) of **5**. NB: this substance is paramagnetic.

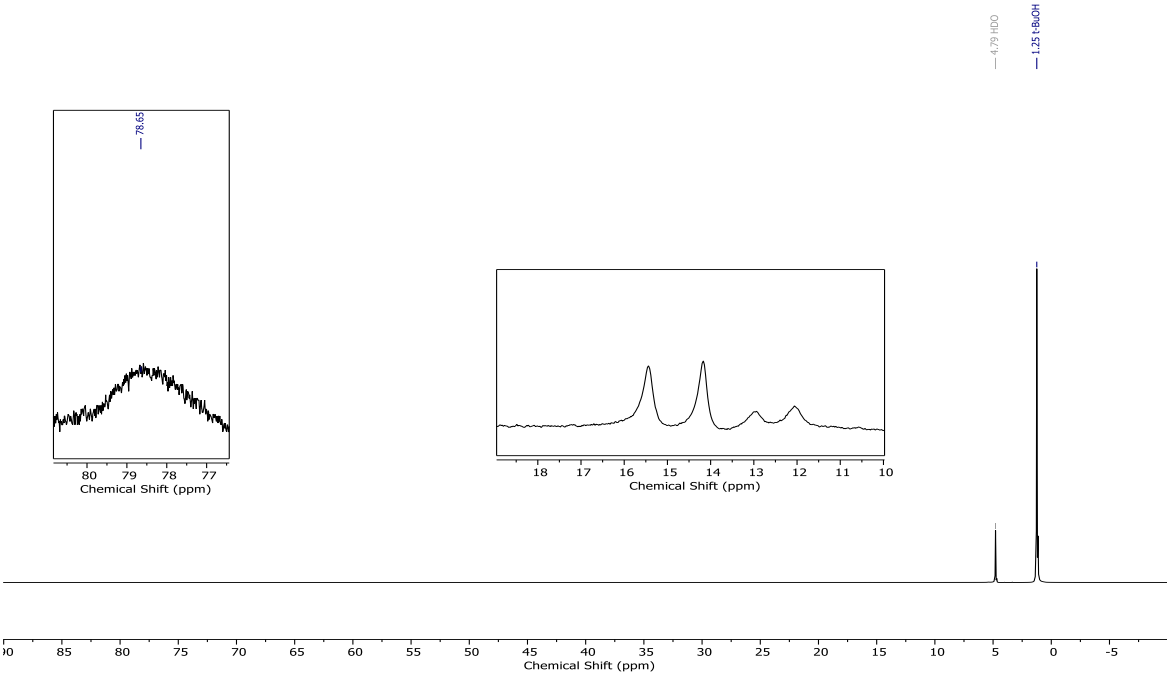

Figure S13. ^{1}H NMR spectrum (500 MHz, D_2O, 10% ^{t}BuOH) of the sample used for Evans' method μ_{eff} determination of **6**. NB: this substance is paramagnetic.

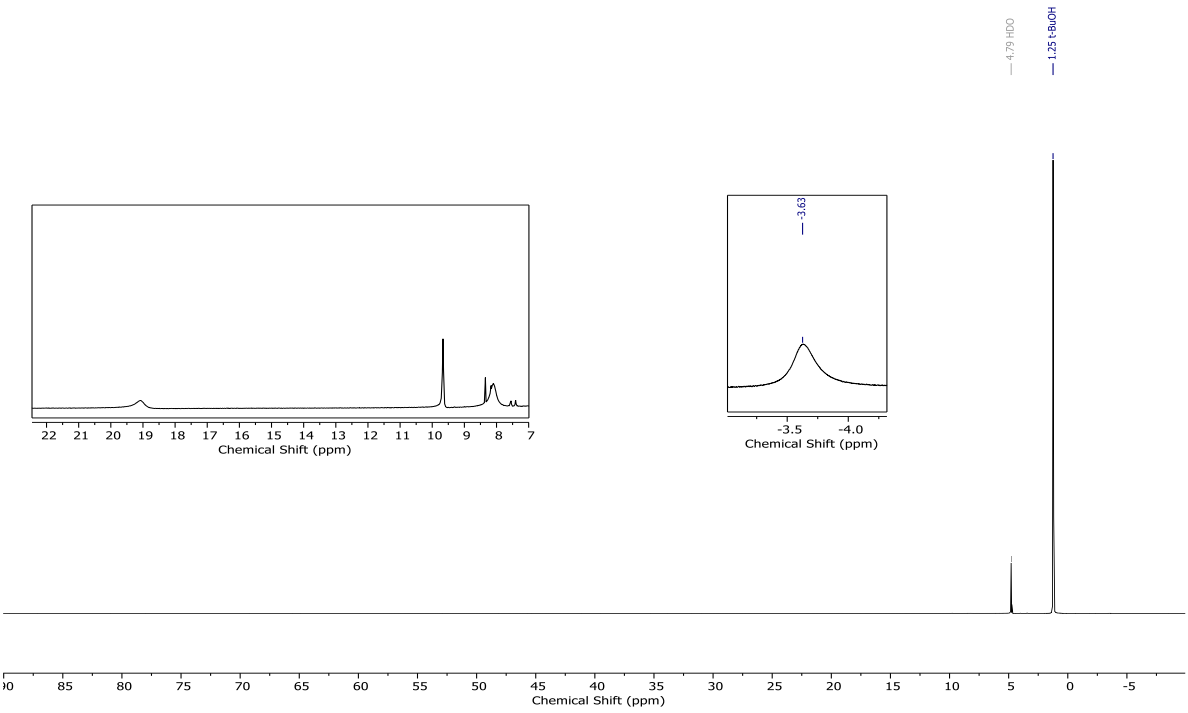

Figure S14. ^{1}H NMR spectrum (500 MHz, PBS-*d*, 10% ^{t}BuOH) of the sample used for Evans' method μ_{eff} determination of reduced **6**. NB: this substance is paramagnetic.

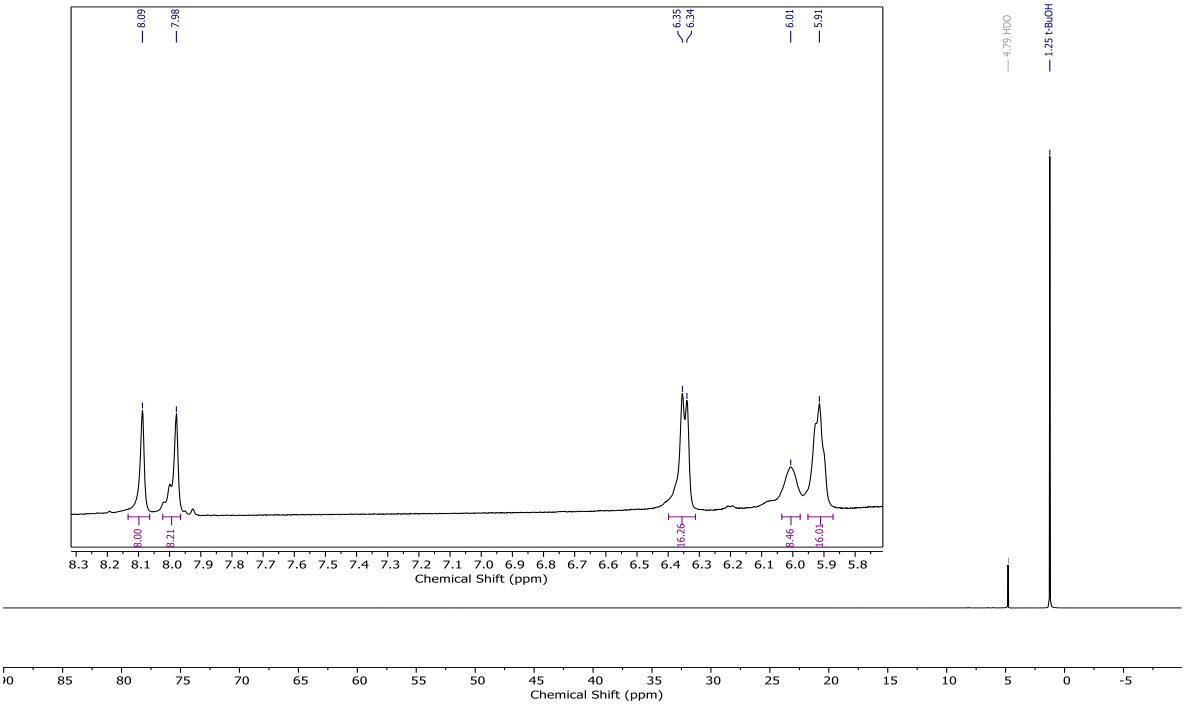

Figure S15. ^{1}H NMR spectrum (500 MHz, PBS-*d*, 10% ^{t}BuOH) of the sample used for Evans' method μ_{eff} determination of **7**.

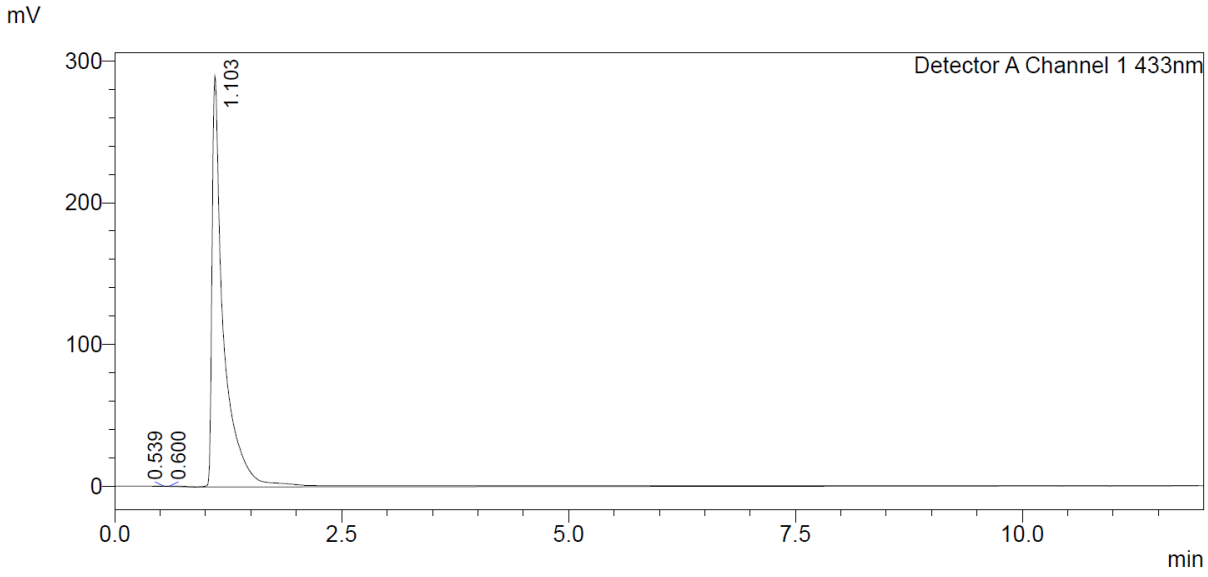

Figure S16. HPLC chromatogram of **6**. Absorbance is measured at 433 nm and the analyte was eluted with a H_2O/MeCN (0.01% TFA) gradient of 0-95% MeCN over 15 min.

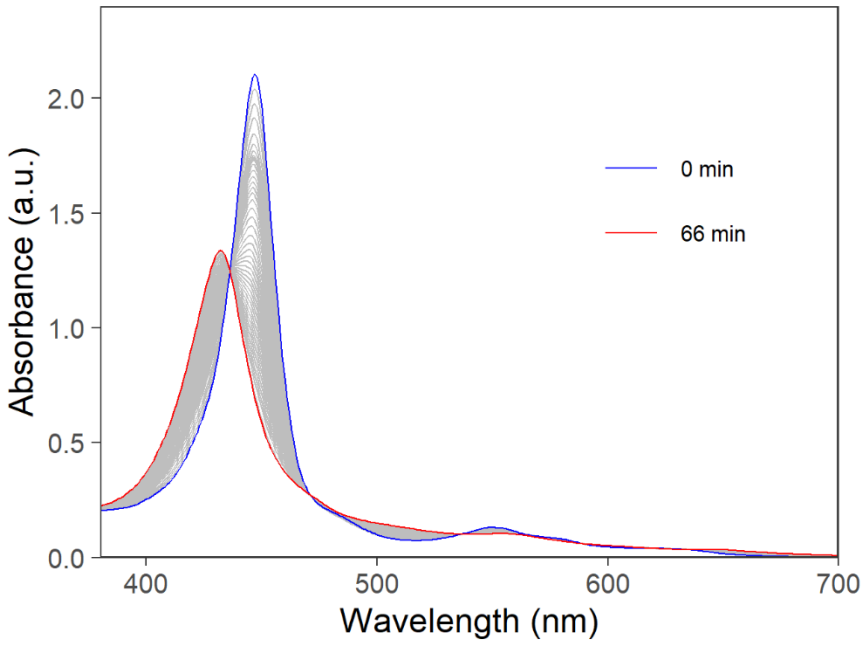

Figure S17. Stability of reduced **6** in PBS (pH 7.4) containing 5.7 mM dithionite following exposure to air. Spectra were acquired at 90 s intervals once dithionite consumption was complete.

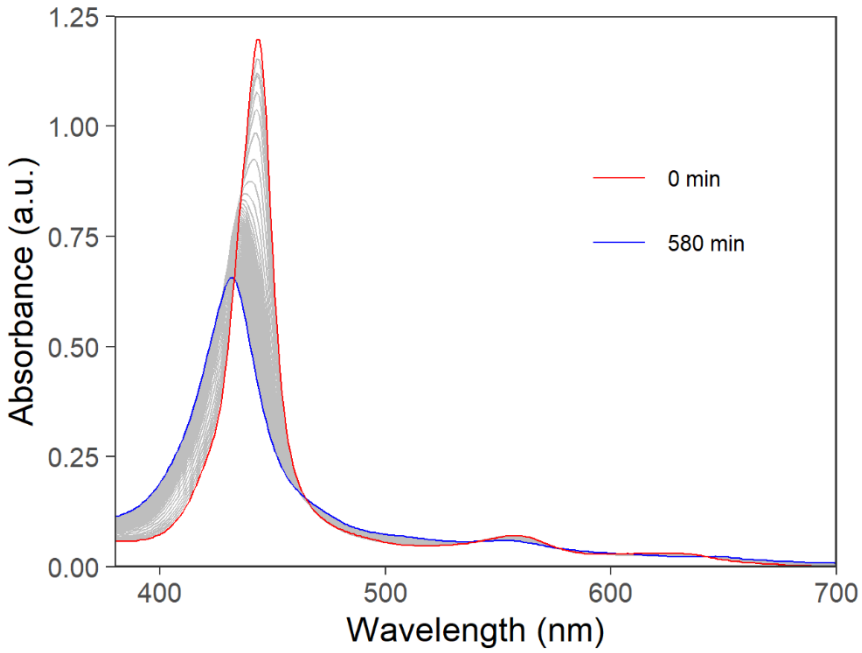

Figure S18. Stability of **7** in PBS (pH 7.4) containing 5.7 mM dithionite following exposure to air. Spectra were acquired at 600 s intervals once dithionite consumption was complete.

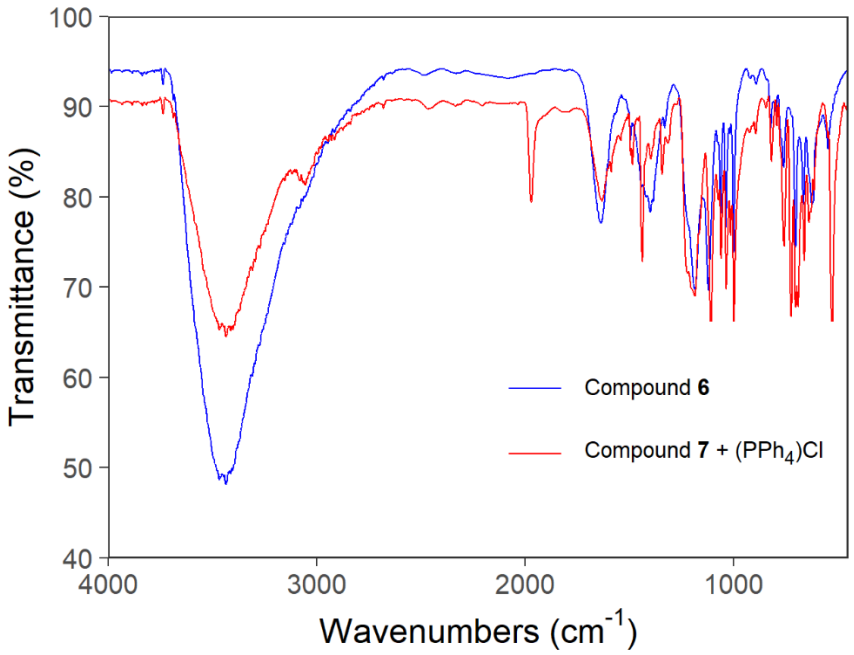

Figure S19. IR spectra (KBr pellet) of **6** and the precipitate formed from **7** and $(PPh_4)Cl$.

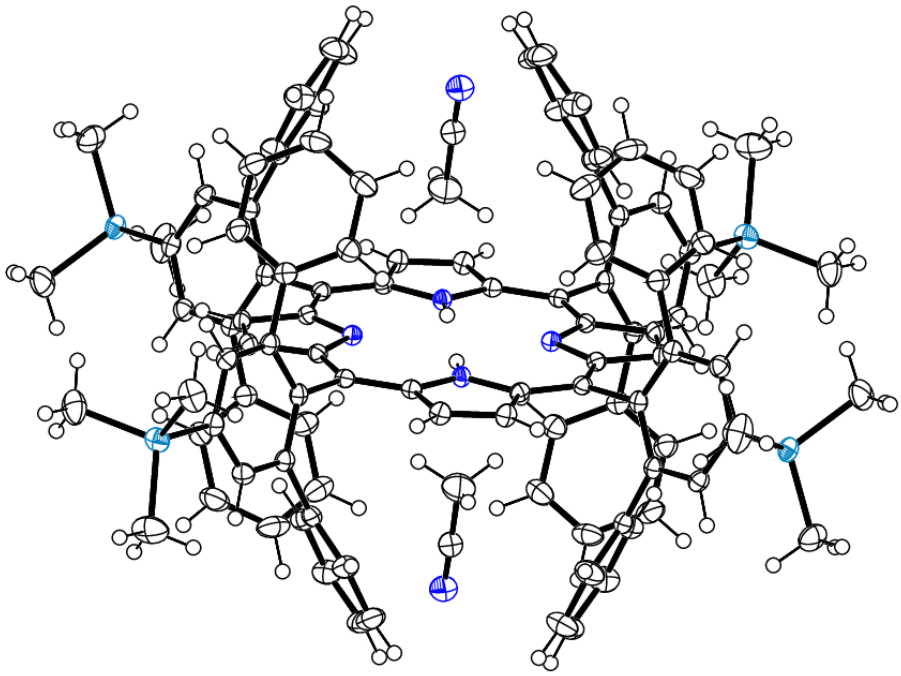

Figure S20. Unit cell contents (50% ellipsoids, H atoms as spheres of arbitrary radius) of the crystal structure of **4**·2MeCN. Disordered H atoms omitted for clarity. Color code: Si teal, N blue, C grey.

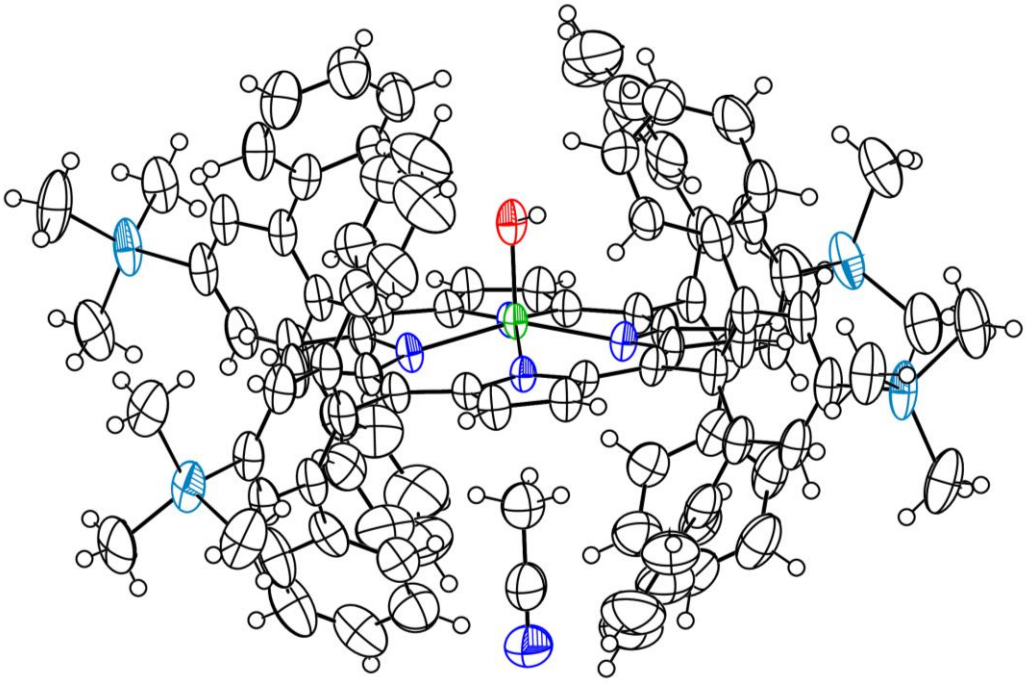

Figure S21. Thermal ellipsoid plot of **5**·DCM (50% ellipsoids, H atoms as spheres of arbitrary radius) from the crystal structure of **5**·DCM·MeCN. Disorder and DCM omitted for clarity. Color code: Fe green, O red, Si teal, N blue, C grey.

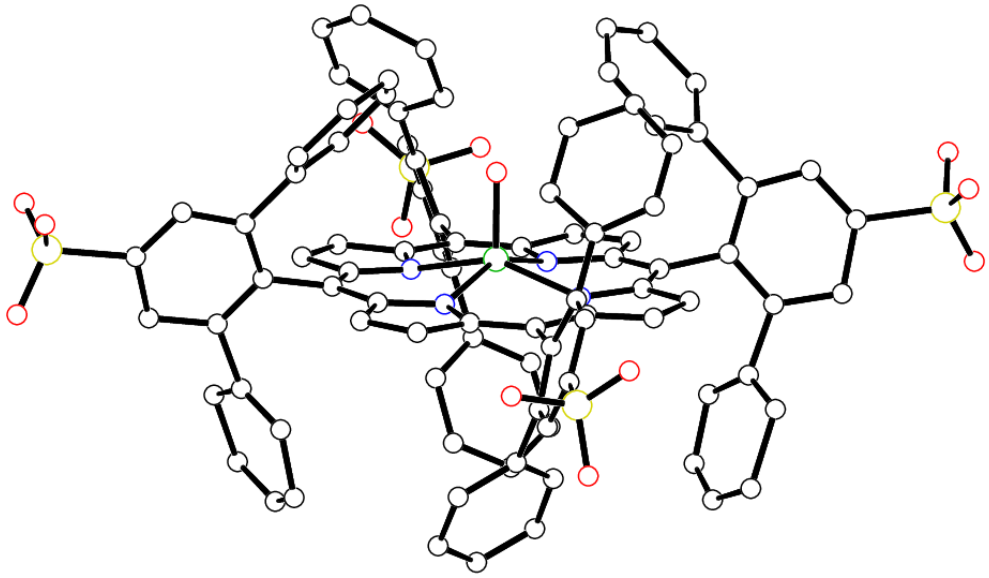

Figure S22. Ball-and-stick representation of **6** from low-quality diffraction data confirming connectivity. Color code: Fe green, O red, S yellow, N blue, C grey.

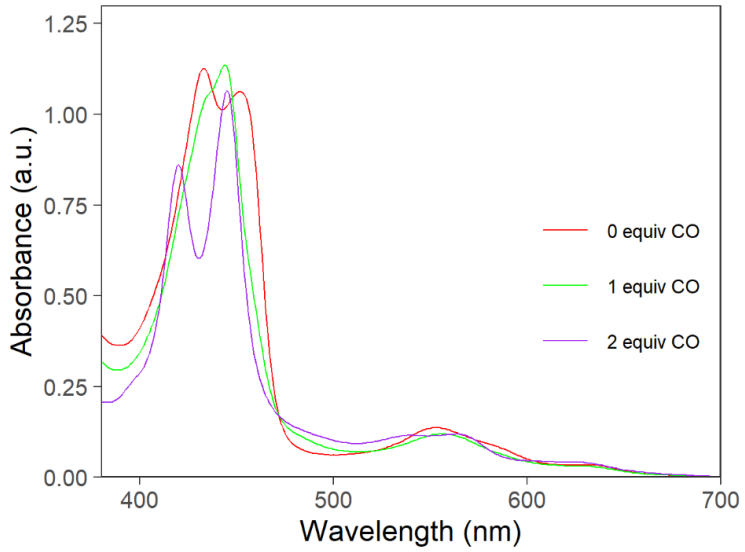

Figure S23. Titration of an equimolar (on the basis of porphyrin centers) mixture of Hb and **6** in PBS (pH 7.4, 5.7 mM $Na_2S_2O_4$) with CO-saturated water. At 0 equiv CO, the mixture contains deoxyHb and reduced **6**. At 1 equiv CO, the mixture contains deoxyHb and **7.** At 2 equiv CO, the mixture contains COHb and **7.**

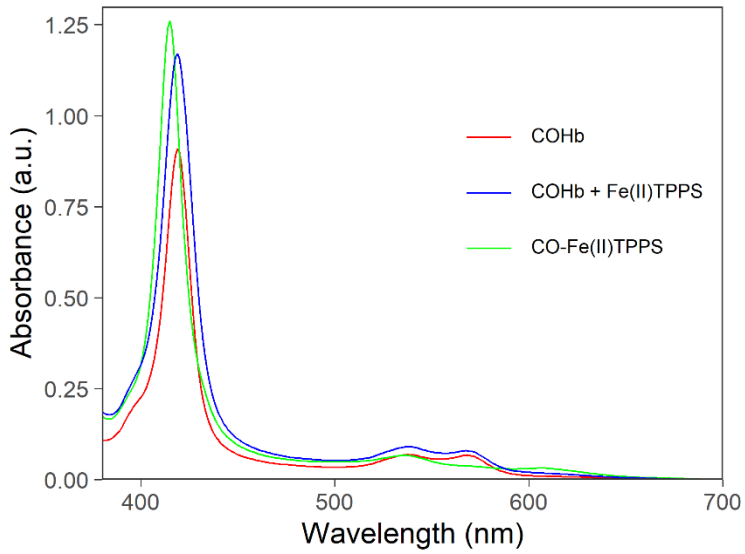

Figure S24. Titration of bovine COHb (2.5 μM) with 1 equiv Fe(II)TPPS (produced *in situ* from reduction of Fe(III)TPPS) in PBS (pH 7.4, 5.7 mM $Na_2S_2O_4$). Also shown is the spectrum obtained when CO is bubbled through a solution of Fe(II)TPPS to form CO-Fe(II)TPPS.

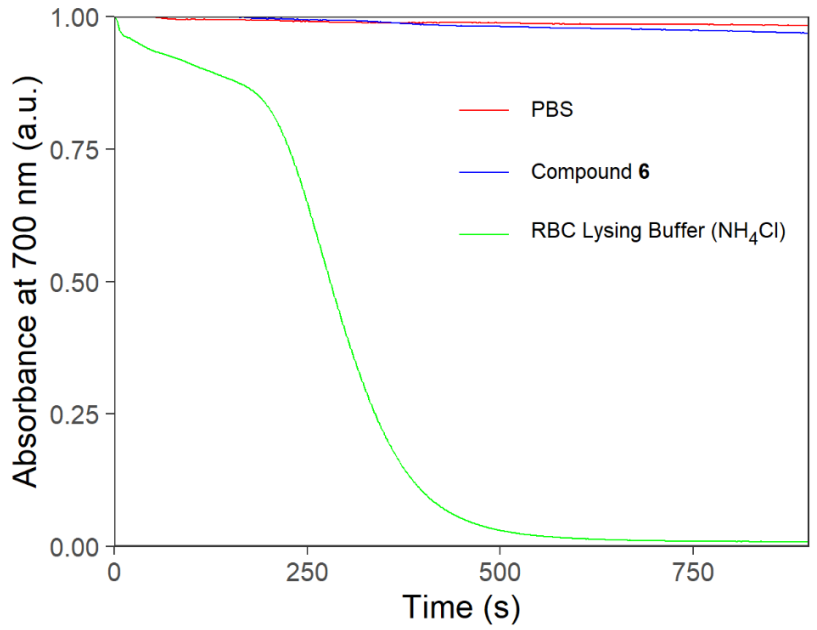

Figure S25. Hemolysis as assessed by measuring OD_{700} over time of a suspension of RBCs in PBS (pH 7.4, 5.7 mM $Na_2S_2O_4$) containing no further additives, an equimolar (on the basis of porphyrin centers) amount of **6**, or 1.5 M NH_4Cl.

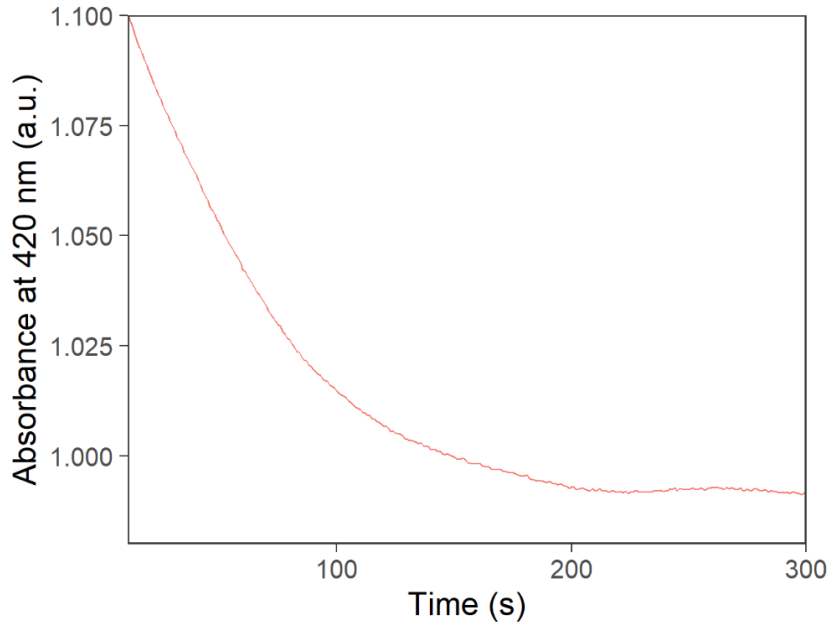

Figure S26. Decrease in COHb (λ_{max} = 420 nm) over time following addition of reduced **6** to a PBS suspension (pH 7.4, 5.7 mM $Na_2S_2O_4$) of CO-treated RBCs at an equimolar amount on the basis of porphyrin centers.

References

1. Adler, A. D.; Longo, F. R.; Finarelli, J. D.; Goldmacher, J.; Assour, J.; Korsakoff, L., A Simplified Synthesis for *meso*-Tetraphenylporphine. *J. Org. Chem.* **1967,** *32* (2), 476-476.

2. Fleischer, E. B.; Palmer, J. M.; Srivastava, T. S.; Chatterjee, A., Thermodyamic and Kinetic Properties of an Iron-Porphyrin System. *J. Am. Chem. Soc.* **1971,** *93* (13), 3162-3167.

3. Esfandiari bayat, Z.; Rahiminezhad, H.; Zakavi, S., Solvent effects on catalytic activity of manganese porphyrins with cationic, anionic and uncharged *meso* substituents: Indirect evidence on the nature of active oxidant species. *Appl. Organomet. Chem.* **2019,** *33* (1), e4678.

4. Schubert, E. M., Utilizing the Evans method with a superconducting NMR spectrometer in the undergraduate laboratory. *J. Chem. Educ.* **1992,** *69* (1), 62.

5. Lin, C.-H.; Tour, J., Hydrogen-Bond-Assisted π-Stacking of Shape-Persistent Cyclophanes. *J. Org. Chem.* **2002,** *67* (22), 7761-7768.

6. Guillerm, V.; Weseliński, Ł. J.; Alkordi, M.; Mohideen, M. I. H.; Belmabkhout, Y.; Cairns, A. J.; Eddaoudi, M., Porous organic polymers with anchored aldehydes: a new platform for post-synthetic amine functionalization en route for enhanced CO_2 adsorption properties. *Chem. Commun.* **2014,** *50* (16), 1937-1940.

7. Lindsey, J. S.; Wagner, R. W., Investigation of the Synthesis of Ortho-Substituted Tetraphenylporphyrins. *J. Org. Chem.* **1989,** *54* (4), 828-836.

8. Suslick, K. S.; Fox, M. M., A Bis-Pocket Porphyrin. *J. Am. Chem. Soc.* **1983,** *105* (11), 3507-3510.

9. Ye, B.-H.; Naruta, Y., A novel method for the synthesis of regiospecifically sulfonated porphyrin monomers and dimers. *Tetrahedron* **2003,** *59* (20), 3593-3601.

10. Walker, F. A., NMR and EPR Spectroscopy of Paramagnetic Metalloporphyrins and Heme Proteins. In *Handbook of Porphyrin Science (Volume 6)*, 2010; pp 1-337.

11. Rigaku Oxford Diffraction *CrysAlis^{Pro} software system*, version 1.171.40.78a; Rigaku Corporation: Wroclaw, Poland, 2020.

12. Sheldrick, G. M., *SHELXT* – Integrated space-group and crystal-structure determination. *Acta Crystallogr. Sect. A* **2015,** *71* (1), 3-8.

13. Sheldrick, G. M., Crystal structure refinement with *SHELXL*. *Acta Crystallogr. Sect. C* **2015,** *71* (1), 3-8.

14. Dolomanov, O. V.; Bourhis, L. J.; Gildea, R. J.; Howard, J. A. K.; Puschmann, H., *OLEX2*: a complete structure solution, refinement and analysis program. *J. Appl. Crystallogr.* **2009,** *42* (2), 339-341.

15. Müller, P., Practical suggestions for better crystal structures. *Crystallogr. Rev.* **2009,** *15* (1), 57-83.